PHILOSOPHICAL TRANSACTIONS OF THE ROYAL SOCIETY A MATHEMATICAL, PHYSICAL & ENGINEERING SCIENCES

Separation and Wake of Pulsating Laminar Flow

T. B. Mezaris, C. Barbi, G. S. Jones and D. P. Telionis

Phil. Trans. R. Soc. Lond. A 1987 **322**, 493-523
doi: 10.1098/rsta.1987.0067

Phil. Trans. R. Soc. Lond. A **322**, 493–523 (1987) [493]
Printed in Great Britain

SEPARATION AND WAKE OF PULSATING LAMINAR FLOW

BY T. B. MEZARIS†, C. BARBI‡, G. S. JONES§ AND D. P. TELIONIS
Virginia Polytechnic Institute and State University, Department of Engineering Science and Mechanics, Blacksburg, Virginia 24061, *U.S.A.*

(*Communicated by J. T. Stuart, F.R.S. – Received* 3 *March* 1986 – *Revised* 10 *February* 1987)

[Plates 1–8]

CONTENTS

This is an experimental study of laminar pulsating flow that passes through separation and is led to a separated region. Detailed information is obtained on all interconnected regions, namely, the approaching attached laminar boundary layer, the immediate neighbourhood of separation, the separated shear layer, the large-scale vortical region of the wake and the outer inviscid flow. The approaching flow is pulsated with frequencies that include the natural frequencies of the wake. Flow visualizations are contrasted with instantaneous and averaged digital data obtained via laser-Doppler velocimetry and hot-wire anemometry. The interaction of the disturbing and natural frequencies is studied. Results are compared with recent theoretical advances. It is found that the amplitude of the imposed disturbance grows sharply in the neighbourhood of separation.

1. INTRODUCTION

Five regions of special character can be identified in separating flows: the approaching attached boundary layer, the immediate neighbourhood of separation itself, the separated free shear layer, the wake, and the outer flow. There is no unambiguous definition for these regions, nor is it possible to find a sharp distinction between them experimentally. The position on the surface of the body where the outer flow ceases to follow the contour of the body and turns away from it has been widely accepted by aerodynamicists as the point of separation. This is the point where the boundary layer detaches from the wall and converts to a free shear layer.

† Present address: 5 Papagou Street, Larissa, Greece.
‡ Present address: Institute de Mécanique des Fluides de Marseille, 1 Rue Honnorat, 13003 Marseille, France.
§ Present address: Fluid Mechanics Branch, NASA Langley Research Center, Hampton, Virginia 23665, U.S.A.

The most obvious and practically most significant feature of the flow in this neighbourhood is the levelling of the pressure distribution. The point where this occurs does not coincide with the point of zero skin friction. No significant pressure disturbance can be observed experimentally at the point where the wall shear vanishes. We thus propose here that separation should be defined as the point where the shear layer abruptly turns away from the wall and not the point of zero skin friction.

It has been demonstrated that the Navier–Stokes equations accept solutions near the point of zero skin friction, which in the limit of $Re \to \infty$ are consistent with the above description. The angle of the zero velocity line, the angle of the separating streamline and the thickness of the boundary layer tend to zero in a distance of order $Re^{-\frac{1}{8}}$ beyond the point of zero skin friction. No abrupt changes occur at the point where the wall shear vanishes. Such theories further predict that, indeed, further downstream of the point of zero skin friction the flow turns progressively away from the wall and the pressure levels off.

For many decades, it was accepted that the vanishing of the wall shear occurs at separation and that this condition can be used as a criterion for the phenomenon. In the past two decades, evidence has been collected (Stuart 1971; Sears & Telionis 1975; Williams 1977; Shen 1978) establishing the fact that this is not true for unsteady flow. It is the present group's opinion, formulated during the past few years of experimental work, that this may not be true for steady flow either. In other words, flow reversal may be embedded at the bottom of an attached and well-behaved boundary layer. Further downstream, phenomena like random wake motion or vortex formation are encountered. This may appear at first inconsistent with mathematical models of separation proposed in the past decade and reviewed most recently (Messiter 1983; Smith 1986). This issue is addressed, among others, in the present paper.

A very important factor that controls the wake formation is the shape of the solid body in the region of the adverse pressure gradient. If the contour of the body diverges very mildly from the direction of the approaching stream, as for example in the case of a slender airfoil at a small angle of attack, then there is very little room for the separating shear layer to develop into large-scale vortices. The effect of the wall is very strong. The free shear layer and the wake behave like a very thick turbulent boundary layer. Established experimental techniques and data-processing methods for turbulent boundary layers can then be employed to study the behaviour of the wake (Simpson *et al.* 1977; Simpson 1977; Simpson *et al.* 1981*a*, *b*; Shiloh *et al.* 1981). If, however, the body contour diverges sharply from the direction of the freestream, then there is room for development of large-scale wake vortices. The free shear layer and the wake vortices can then be distinguished from one another. The 'abrupt turning' of the outer flow away from the wall may become more obvious.

In view of these considerations, the five regions near separation can be defined as follows (see also figure 1). (I) The approaching attached boundary layer, which may contain a thin region of reversed laminar and very slow moving flow. (II) The immediate neighbourhood of separation downstream of which wake properties become apparent and the outer flow turns away from the wall. At separation the shear layer lifts off the wall and separates the next two regions; it is not yet a free shear layer because of its proximity to the rigid wall but not far downstream, it becomes (III) a true free shear layer. (IV) The wake is the region of 'dead air', where the flow is slow, vortical but random in character. (V) The outer flow. This idealized distinction of course is not always possible, because further downstream, the free shear layer rolls up and mixes with the wake bringing in it momentum from the outer flow. Moreover,

PHILOSOPHICAL TRANSACTIONS OF THE ROYAL SOCIETY A MATHEMATICAL, PHYSICAL & ENGINEERING SCIENCES

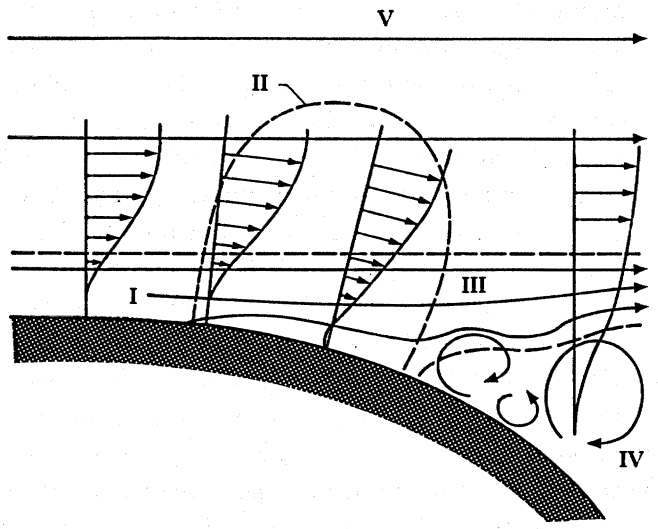

FIGURE 1. Schematic representation of separating flows.

flow in the far wake can not be characterized as 'dead', because velocities in it reach levels comparable to the speed of the outer flow. Smith (1977) used very similar notation and identifies three regions with Roman numerals. His outer flow, separated region and free shear layer are identified by the symbols I, II and III, respectively.

In most of the analytical efforts, these five regions have been investigated independently or, at most, two at a time. However, the past decade has seen impressive breakthroughs in this area, starting with the development of the triple-deck theory (Stewartson 1974). For subsonic flow leading to massive separation, significant contributions were made by interacting the local description with a Kirchhoff solution for the outer flow (Sychev 1972, 1979; Smith 1977, 1979, 1985*a*; Messiter 1979). Discussion of these analytical efforts and a more complete account of contributions can be found in recent review articles (Messiter 1983; Smith 1986).

Experimental works focused on certain regions of the flow; others examined the problem via either a very large or a very small scale of reference. As a result, useful information on one of the regions could not be coupled with data in another region. For example, detailed boundary-layer data were not accompanied with free shear layer data, or wake properties, and vortex sheet roll-up characteristics were not connected with the features of attached boundary layers that develop upstream of separation. In this paper we report on our experimental efforts to define a problem and devise methods of measurement that would give a global picture of the phenomena involved.

Regions I and II (figure 1), namely the attached boundary layer and separation, have been investigated extensively in the past, although the interest in unsteady separation has been brought to the attention of investigators only in the 1950s. Many theoretical investigations were mostly concerned with the behaviour of the boundary-layer equation in the neighbourhood of unsteady separation and its ability to predict the phenomenon; see reviews by Shen (1978) and Telionis (1979). In all the contributions described in these references no effort is reported for coupling the wake flow properties to the attached flow. In other words, no feedback is provided from the unsteady wake to the approaching stream.

Region III, namely free shear layers, has received a lot of attention in the past, but only

for very simple flow configurations. In most cases, two uniform streams with different speeds were suddenly brought into contact. Mixing of the streams has been a main concern, and most of the experimental work concentrated on roll-up of the shear layer and the coherent structures that develop. Some recent representative works are reported by Brown & Roshko (1974), Winant & Browand (1974), Corcos & Sherman (1976) and Browand & Weidman (1976). A thorough review of this topic can be found in Ho & Huerre (1984). The free shear layer that emanates from the point of separation has not been examined in the light of such recent results on mixing layers. It has been known that at least the first stages of the shear layer roll-up may be analytically investigated via linear stability theories (Michalke 1972). With the exception of Smith (1985), this approach has also been ignored in the study of separating flows. The present group (Jones *et al.* 1981) obtained flow visualizations of circular-cylinder wakes, clearly indicating the formation of instabilities along the separated free shear layers. Most recently, Smith (1985) examined various types of instabilities that can be triggered off in the neighbourhood of separation and pointed out that the structure of such separation is exactly the same as the structure of Tollmien–Schlichting instabilities (Smith 1979).

Regions IV and V, namely the potential flow about a blunt body and its wake and the vortical wake region, have received very little attention by theoreticians. Wakes are modelled most efficiently by releasing discrete potential vortices in the flow (see, for example, Katz 1981 and references therein). An elegant approach can be found in Smith (1979, 1985*a*) who actually identifies regions similar to those of figure 1. However, his analysis is confined to high Reynolds numbers and his wakes are steady and have finite lengths.

What emerges here as a novel approach to the problem of wake formation is to view the separated free shear layer and the wake vortices as two separate elements of the wake and study their possible interaction. The question is posed as follows: is it the natural frequencies of the free shear layer that control and drive the large-scale wake vortices, or is the free shear layer just the edge of the wake therefore behaving as a containing boundary? We attempt to provide an answer to this question here, and in Jones *et al.* (1981), where we examine the wake of a circular cylinder. The wake of a cylinder contains both positive and negative vorticity, generated from the two separated free shear layers. The test model in the present paper is one sided and therefore there is no interaction between the two free shear layers and large-scale vortices of opposite sense. The problem considered here is closer to flow separation over the suction side of an airfoil at an angle of attack.

The brief review of the theoretical work provided here clearly indicates that progress has been made for analysing separately the different regions of separating flow. The experimental effort in this area has not been appropriate for comparison with the theory. It appears that communication between theoreticians and experimentalists has not been adequate. Some excellent experimental work has been published on the topic. Investigating flows about airfoils, Ruiter *et al.* (1971), Carr *et al.* (1977) and Maresca *et al.* (1976) provided evidence that in oscillating flows, thin reversed layers may shoot periodically upstream of separation. However, these efforts were centred around the phenomenon of unsteady stall *per se*, and provided little information about the boundary layer and the point of separation.

A careful experimental investigation of oscillating laminar boundary layers was reported in Hill & Stenning (1960). A decelerating outer flow was introduced leading to separation, but measurements were not obtained near separation. The first detailed report on oscillatory separating laminar boundary layers appeared much later (Despard & Miller 1971). In this

paper, Despard & Miller provided detailed data for a boundary layer over an airfoil-like body. Periodicity was introduced in the mean flow by a system of shutters. This work is most relevant to the present investigation and the methods and results reported in it will be discussed in more detail in the main body of the paper.

Most recently, Varty & Currie (1984) reported detailed laser-Doppler velocimetry (LDV) measurements around a circular cylinder with emphasis on laminar separation. However, only steady-flow data were presented. Didden & Ho (1985) studied unsteady separation generated by the passage of ring vortices over a flat-wall boundary layer. They were thus able to capture a separation moving upstream in a phase of a periodic motion.

Experimental investigations of transient laminar separation were reported by Telionis & Koromilas (1978) and Koromilas & Telionis (1980). The work was conducted in the VPI water tunnel, a facility designed and constructed especially for this project. A flow-visualization method was developed and a brief description follows again in the present paper. Koromilas & Telionis allowed a boundary layer to develop on the bottom wall of the water tunnel and led it over a hump with a circular arc profile to induce separation. Their disturbances were introduced downstream and they were mostly transient in character. Oscillating separating flows were also reported by Koromilas & Telionis (1980) but results were rather limited and the information inconclusive. The present paper is a continuation of this effort, with a slightly different model and disturbing mechanism but the same methodology and the same range of Reynolds numbers.

In the study of unsteady separating flows, it is essential to detect the size and shape of the wake. Despard & Miller (1971) were able to detect large disturbances in the outer flow that they interpreted as the beginning of the wake. However, they provide no actual data on this information and no detailed results beyond separation. The present investigation is based on a reliable method of flow visualization that reveals the instantaneous direction of the streamlines in the entire flow field. The experiments of Despard & Miller were conducted in a wind tunnel, and hot-wire anemometry was used to obtain the data. The experiments described here were performed in a water tunnel. Laser-Doppler velocimetry, as well as hot films, was used for measurements. As a result, it was possible to examine a range of reduced driving frequencies beyond the range of frequencies considered by Despard & Miller.

Our goal here is to study the response of separating flow to periodic external disturbances. We search for the response of the velocity field, namely the fluctuating components, that vary with the same frequency of the external disturbance. However, to provide a more complete picture of the flow, higher harmonics of the disturbing frequency, the natural frequency and its higher harmonics and possible couplings have been also considered. Detailed LDV measurements were obtained both upstream and downstream of separation. These results are accompanied with dye and particle visualizations.

In the following two sections we discuss in detail the experimental facilities and instrumentation used in this research. The test model and the experimental rig are described in §4. In the same section we also provide and discuss results for the response of the outer flow to the external disturbance as well as information on the steady and mean boundary layer and separation.

Sections 5 and 6 are the heart of the paper. They contain results on the unsteady motion, the free shear layer and the separated region. Finally, a critical review of our findings and comparison with other results reported in literature is given in §7.

PHILOSOPHICAL TRANSACTIONS OF THE ROYAL SOCIETY A MATHEMATICAL, PHYSICAL & ENGINEERING SCIENCES

2. Experimental facilities

Experiments were conducted in the VPI water tunnel. This facility is described in detail in Telionis & Koromilas (1978) and Koromilas & Telionis (1980). The tunnel has test-section dimensions of 25 cm × 30 cm, and achieves velocities up to 3 m s^{-1}. Two sets of coarse honeycombs are situated in the settling chamber but no screens can be used there. This is because visualization particles are then trapped and block the flow. To improve the quality of the flow for this study, a third honeycomb was located immediately downstream of the converging section followed by two fine sets of screens that can be removed and cleaned periodically. The turbulence level was measured again recently, after elimination of high-frequency optical and electronic noise and was found to be less than 0.5%.

Minor and recent modifications of the tunnel, for example the installation of airfoil sections over supporting struts, automatic temperature control units, are described in detail in Jones (1980). In the same reference, a report is given on a detailed vibration analysis, which revealed that the test-section panels are virtually free of vibrations and that the signals from accelerometers and laser velocimetry are totally incoherent.

Three systems of sensing devices were used: a laser-Doppler velocimeter (LDV), a hot film (HF), and flow visualization. The first two provide instantaneous point measurements whereas the third generates average velocity fields. Simultaneous measurements and flow visualization were obtained selectively. For the laser measurements, a Disa one-channel system (55L series) was used, as shown in figure 2. The forward-scattering mode was selected; in this mode, the light scattered by the particles has the highest intensity thus improving the signal: noise ratio. A 5 mW helium–neon laser (Spectraphysics model 120) directed a laser beam through the beam splitter (55L01 series). A system of Bragg cells was attached on the casing of the beam splitter to provide for frequency shifting. The photomultiplier (55L10) was positioned in the bisector plane of the two beams. The signal generated by the photomultiplier was led to a preamplifier (55L30) followed by the frequency tracker (55L30) and a signal processor (55L40).

The component of velocity in the plane of the two beams and in the direction perpendicular to their bisector was thus measured. The relation between this component of the velocity and

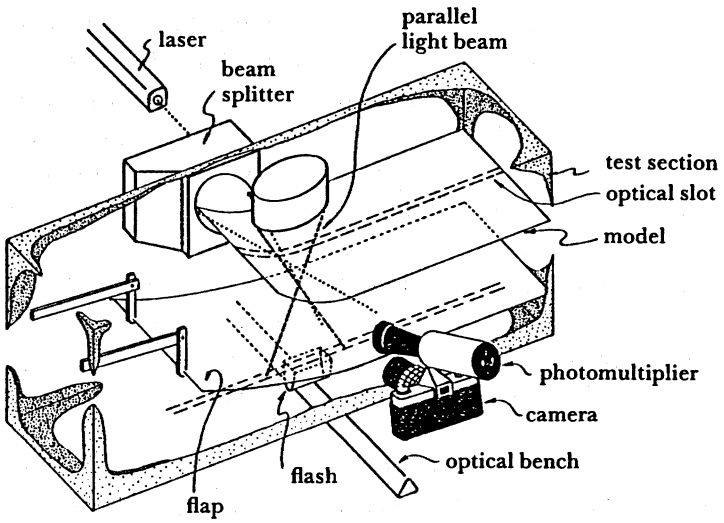

Figure 2. Experimental arrangement.

the Doppler frequency, δ_D, for the differential mode is $v = \delta_D(\frac{1}{2}\lambda)\sin\frac{1}{2}\theta$, where λ is the wavelength of the laser beam and θ is the angle between the two beams. To measure the velocity component parallel to the boundary in the adverse pressure gradient region, two inclinations were given to the plane, p, of the two beams as shown in figure 3. At first, the plane was inclined by an angle β with respect to the horizontal, to become parallel to the tangent at the station of measurement. Then the plane was rotated about the point of measurement, M, retaining its bisector plane, r, fixed. The bisector line is thus given an inclination α with respect to the generator of the model surface. This permits measurements in the immediate neighbourhood of the wall.

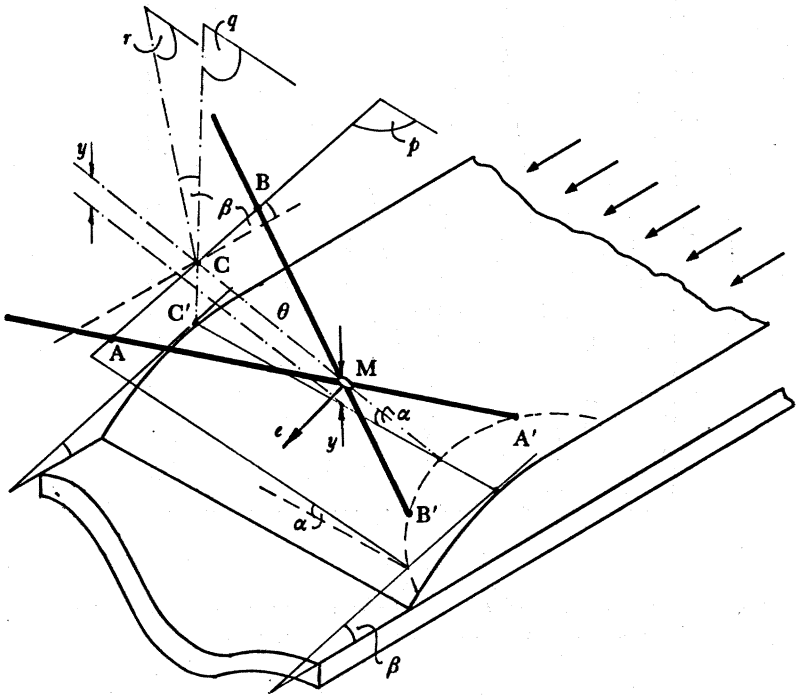

FIGURE 3. Angles involved in laser anemometry.

The hot-film measurements were performed with a Disa 55D series anemometer and a 55R15 boundary layer probe. This probe consisted of a nickel-plate tungsten wire of diameter 70 μm with an overall length of 3 mm and a sensitive film length of 1.25 mm. A Disa 55D01 constant-temperature anemometer was operated with a bridge ratio of 1:20, with a cable length of 5 m. The anemometer output voltage V was related to the water velocity U by $V^2 = V_0^2 + BU^n$, where V_0, B and n are functions of temperature. All anemometer outputs were processed in the Disa 55D10 linearizer.

The laser system was traversed in two directions on a lathe bed as described in Mezaris (1979). A traversing mechanism with two degrees of freedom was specially designed and constructed for traversing the hot film. A Slo–syn stepping motor control system (model SP 153) was used to traverse the hot film with steps of 2.5×10^{-3} cm in the x-direction and 6.3×10^{-4} cm in the y-direction.

Measurements with the Bragg cells in the region of the recirculating bubble were obtained but after three of four cycles, the tracker detuned. This was caused by poor seeding, which becomes quite important in the immediate vicinity of the wall, and a deficiency in the design

of the tracker. Both deficiencies have since been corrected with appropriate seeding (Polymerics XPR-143) and special 'recapture circuitry' added to the tracker. With no Bragg cells the negative forms of the instantaneous wave form appear inverted. A typical time record for two periods is shown in figure 4. In this and some other figures that follow, only the direct reading of instrumentation is presented. The Bragg cells were used to verify this fact. Most of the measurements were then taken with no Bragg cells.

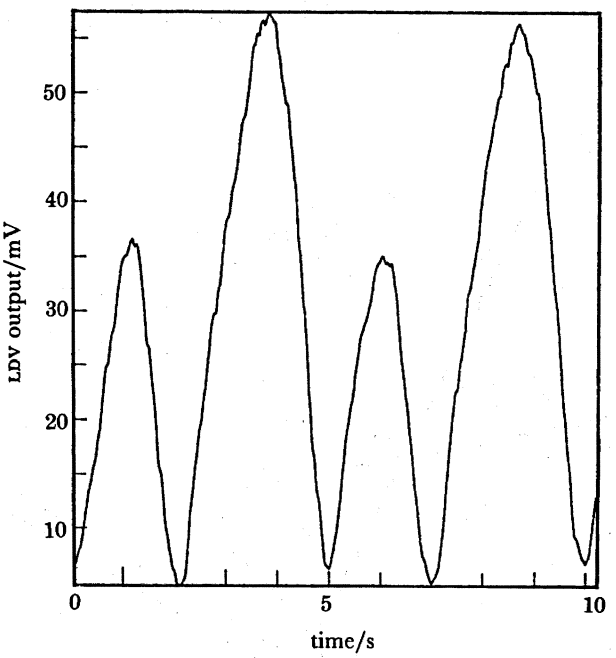

FIGURE 4. Example of an averaged time record at a point where the flow is partly reversed showing the negative portions of the instantaneous velocity inverted.

Flow visualization was used to obtain an overall picture of the flowfield. The technique is the same as that of Telionis & Koromilas (1978) and Koromilas & Telionis (1980). Pliolite particles of 0.1–0.2 mm diameter having excellent scattering features were dispersed in the medium. The pliolite particles have specific density 1.02 and indicate an almost neutral buoyancy behaviour in the water. A thin sheet of light passing through a slot of the model illuminated the particles as they moved with the flow as shown schematically in figure 2. If the time of exposure is much smaller than the time constant of the unsteady phenomenon under observation, then the small path segments exposed on the film are approximately tangent to the instantaneous streamlines and their lengths are proportional to the instantaneous value of the velocities at the mid-points of the paths.

A Nikon camera with a focal-plane type shutter was used to obtain still pictures. The camera can give up to five frames per second and an f-stop equal to 1/8 was used. When calculating the velocity field from the pictures, correction of the exposure time was made because the moving particles are exposed for larger or smaller time interval, according to their velocity and direction of motion with respect to the direction of motion of the shutter (Telionis & Koromilas 1978).

The flow was also visualized with dyes emitted on the skin of the model. The dye-supply head was carefully controlled to avoid interference of the dye jet and the flow.

3. Data acquisition and calibration

The data obtained by the laser-Doppler velocimeter (LDV) or the hot film (HF) were reduced digitally. Two systems were used interchangeably: a Zonic fast Fourier transformer (DMS 5003) and a Hewlett Packard signal analyser (HP-5420). A block diagram showing the two systems is given in figure 5. The two-channel data memory system (DMS) of the Zonic is a transient recorder system that performs local analysis in both the time domain and the frequency domain. The DMS 5003 is classified as a software-controlled data-acquisition system with analysis, display and communication capability.

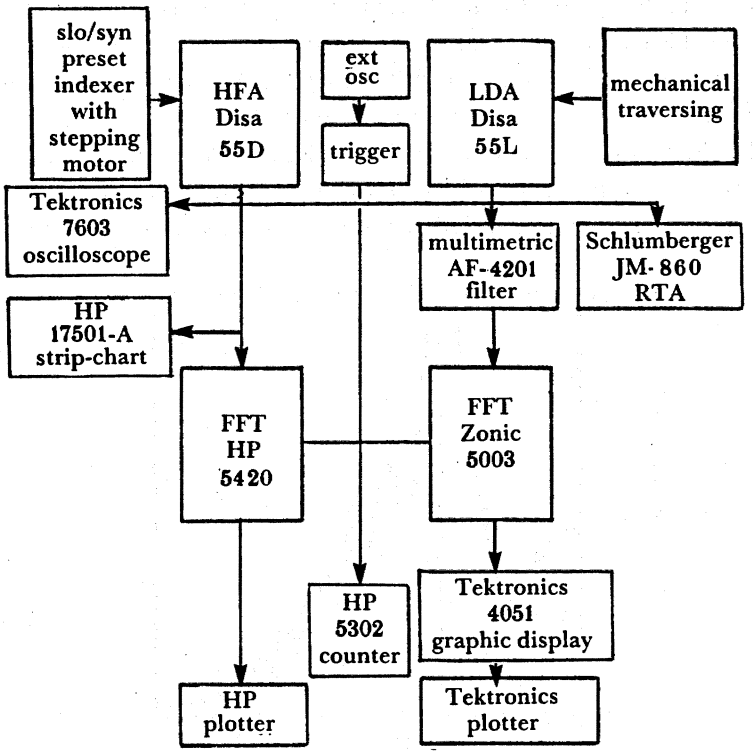

Figure 5. Block diagram of VPI and SU water tunnel data-acquisition system.

The Zonic–FFT requires external filtering of the LDV or HF signals. This is due to aliasing. A filter with a high attenuation slope, 48 dB per octave, was used (Multi-Metric Inc., model AF-420L). The HP 5420A signal analyser is also a two-channel digital instrument that provides time and frequency domain analysis of analogue signals in the range 0–25 kHz. Analogue data are input through the HP 54410A analogue/digital converter, and anti-aliasing is provided by a HP 54470 digital filter.

It should be emphasized that the principles of operation of the LDV and the HF are totally different. Moreover, the electronic hardware necessary to convert the original information to a voltage is also completely different. Matching of the two signals obtained by the two methods at the same point in the flow is almost perfect (Jones 1980).

The data were ensemble averaged. Both 'free-run' and 'external triggering' were used for conditional sampling. The external trigger was controlled by an LED that senses the revolutions of the mechanical oscillator.

Preliminary tests were conducted to estimate the necessary number of time records for ensemble averaging. This is essentially connected with the repeatability of the phenomena under investigation. These phenomena are very complex, because they are neither deterministic nor purely random. It is true that the eddies that are generated in the wake are large, sometimes the order of the thickness of the wake, and they appear well organized; their activities of growth and downstream motion follow a certain pattern. Yet their size and the period of shedding are 'semi-random' quantities.

The necessary number of samples for a reliable signal is not easy to define. However, we are confident that 15 or more give consistent results. It was discovered that when 30 or more averages were taken, the broad-band noise was reduced in amplitude, but the observed signal would only slightly decrease and broaden. In the wake regions, the number of averages was limited to the time the LDV would consistently track. Spectra of the signals at a point along the free shear layer, obtained during two different time intervals and averaged 20 times only are shown in figure 6. The driving frequency was 0.6 Hz; this and its harmonics were reproduced both times fairly accurately. There is some discrepancy in the amplitude of the peaks; however, this is less than 5%. Whenever the amplitude was not of major concern, data were obtained with 15 averages. Otherwise, 20 or more ensemble averages were taken.

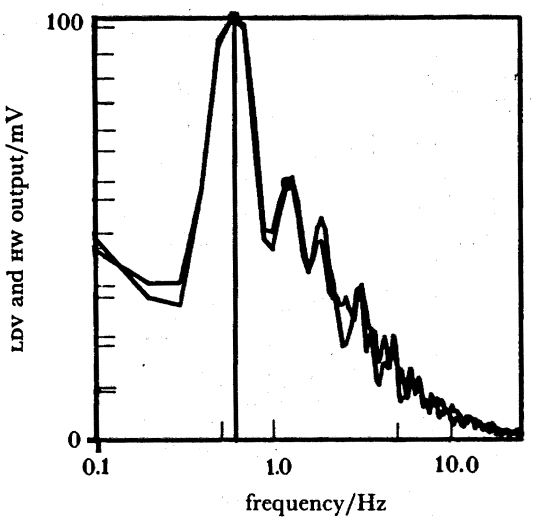

FIGURE 6. Spectra obtained by the hot film at the same point but during two different time intervals at a driving frequency of $f_d = 0.6$ Hz.

4. THE MODEL AND THE BASIC FLOW

In this section we provide experimental data for the undisturbed flow over the model. Detailed data for the entire region between the two flat plates, as, for example, mean profiles in the streamline or spanwise directions, and turbulence levels, have been included in Jones (1980). Here we concentrate our attention on the undisturbed flow in the region of adversed-pressure gradient. The response of the flow to external periodic disturbances will be discussed in the following two sections. However, even with steady outer flow conditions, the flow is inherently unsteady, because of the natural unsteadiness contained in the wake. We also include here information on the response of the potential flow to periodic disturbances induced

by the oscillating flap, namely region V of figure 1. This should be the necessary boundary condition for calculations of the viscous flow. No attempt was made to reduce the frequency of the disturbance. Theoreticians may want to choose typical quantities from the available lengths and velocities to define a dimensionless frequency.

Experiments were performed on the model shown in figure 7. The flow was led into the test section from the right and into the region of zero pressure gradient between the two flat plates ED and IK. A slight divergence of the plates was introduced to account for the thickening boundary layers at a Reynolds number $Re = 1.5 \times 10^4$ based on the equivalent length of a flat plate. A region of adverse pressure gradient was generated between the cylindrical surface EF and the flat plate GH. The plate GH was connected to the flat plate IK through the flexible surface HI and was free to rotate approximately around point I. Rotation of the flat plate GH changed the distribution of the adverse pressure gradient in this region. The flow separated at some position on the surface EF. The position of the plate GH was thus controlling the location of separation on the surface EF.

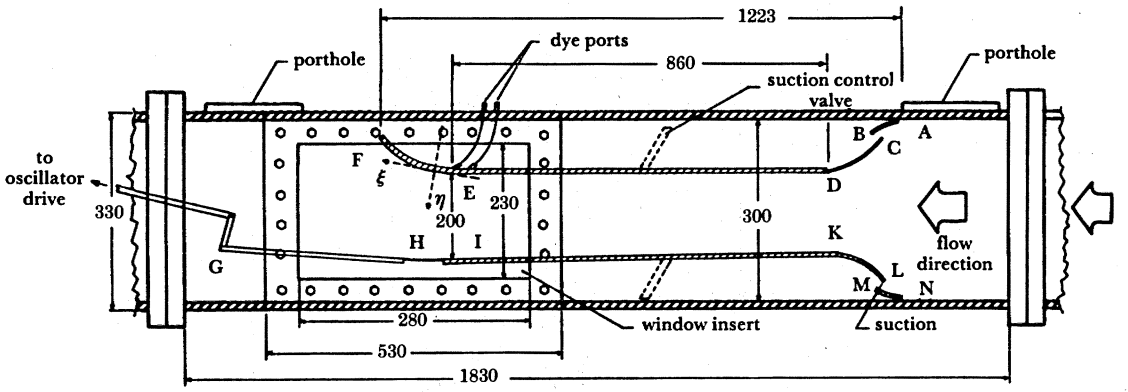

FIGURE 7. The model mounted on the test section. All measurements are given in millimetres.

To insure that a laminar boundary layer was at hand, the wall layer at the leading edge of the model was removed. This was accomplished by suction through the slot formed between the cylindrical surfaces, AB and CD. Flow visualization showed that all the boundary layer of the wall was removed and the approaching flow was laminar. The same construction was used to remove the boundary layer of the lower wall of the tunnel before the flow reached the flat surface IK. The small convergence CD and IK therefore served two purposes. It provided a simple method for removing the wall boundary layers, and it led the flow downstream of the fine honeycomb and screens through a second convergence that reduced further the freestream turbulence.

The described model was expected to generate a time-independent flow between the two plates with unsteadiness confined downstream of the station E. It turned out that flap disturbances mildly influence the mean flow as well. This was attributed to heavy loads on the impeller and the pump. These loads force the pump to operate at the lowest portion of its discharge capacity, a region very sensitive to changes in the total head. Moreover, it appears that the suction method introduces periodic circulation around each plate and thus superimposes a small fluctuating component to the mean flow. The quality of the flow between the two plates has been documented (Jones 1980) and will be briefly discussed later. A much more

effective method for generating steady flat plate flow that leads into a region of fluctuating adverse pressure gradient has been employed by Parikh *et al.* (1981). The present method could actually be improved if controlled bleeding were to be effected at BC and ML by a separate circuit.

The surface EF on which separation occurs has a circular arc profile and a radius of 22.8 cm. It is made of a Plexiglass frame on which a transparent Lexan plate was glued. The outer surface of EF was coated with black fume except for a 5 mm strip in the streamwise direction that was used to generate a flat sheet of light. Measurements were obtained on the upper surface of the duct that is next to the wall DEF. A detail of the portion EF of the model is shown in figure 8. This is shown inverted, and the flow in this orientation is moving from left to right. All flow visualizations in this paper are oriented as in figure 8. In this figure we have also shown the cross sections of two supporting rods. Viewed from a point approximately along their axes, the size of their cross section is exaggerated in the flow visualizations that follow. This is because the camera was always focused in the middle of the test section. However, their relative distance can be used as a convenient length scale.

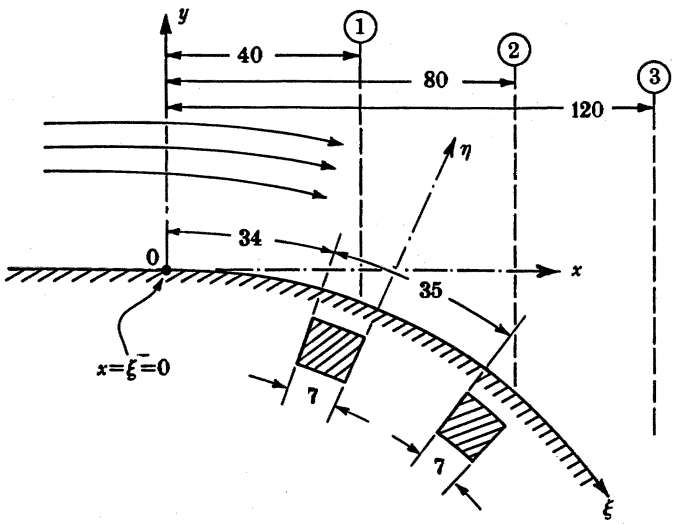

FIGURE 8. The aft part of the model, i.e. the circular arc EF of figure 7 in an inverted position.

The origin of the coordinate systems x, y and ξ, η is at the point where the flat surface DE joins the circular arc EF. The system x, y is aligned with the direction of the flow whereas the system ξ, η follows the contour of the body. The first is more appropriate or studying the free shear layer and the second for studying the vortical motion in the wake. In the first type of measurements, the laser-beam plane was always horizontal to measure the component of the velocity in the direction of the approaching stream. In the second type of measurement the laser-beam plane was rotated to be tangent to the surface of the body at the station of measurement. This is a distinct advantage of LDV against HF.

Detailed calibration of the flow between the flat plates, namely velocity and turbulence intensity profiles in both transverse directions, are reported by Jones (1980). The boundary-layer profiles collapse on the flat-plate Blasius solution within an error of about 3% of the freestream velocity. Apparently, the effect of the small curved entrance is negligible and the flow between the two flat walls is very nearly a flat-plate laminar boundary-layer flow. The

turbulence intensity varies between 0.3 and 0.5%, depending on the location and tunnel speed. The mean flow is essentially uniform between the two plates but a weak fluctuating component is superimposed. The amplitude of the oscillation does not vary with axial distance; data are presented in figure 9 only for the last portion of the flat plate, but detailed investigations (Jones 1980) indicated that this is true for the entire length between the two plates.

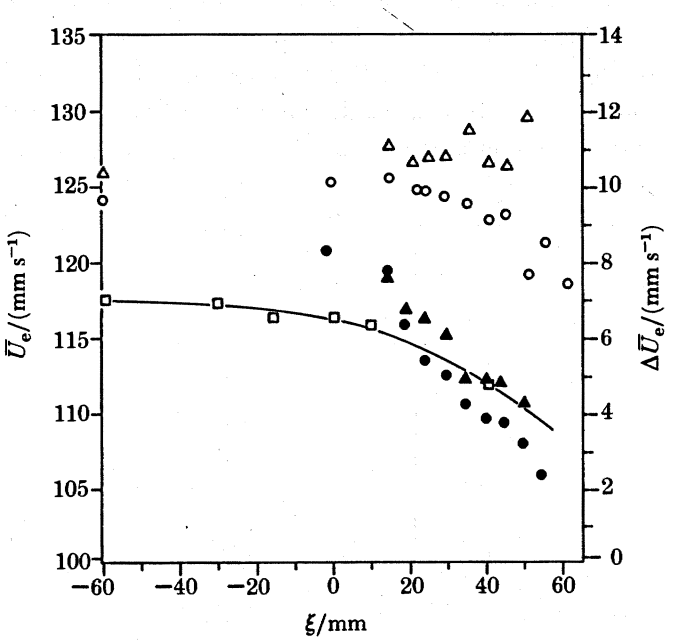

FIGURE 9. Outer-flow velocity distributions. Symbols: □, steady flow, $U_e(\xi)$; ○, $f_d = 0.2$ Hz, △, $f_d = 0.5$ Hz, unsteady flow mean distribution, $\bar{U}_e(\xi, t)$; ●, $f_d = 0.2$ Hz, ▲, $f_d = 0.5$ Hz, unsteady flow amplitude, ΔU_e.

The extreme positions of the flow-reversal point for the upper and lower position of the flap, GH, were respectively $\xi = 36$ and 61 mm. The two positions of the flap, namely the lowest and highest, will be referred to in the sequel as positions I and II, respectively. The velocity distribution along the ξ-axis in the steady-state case and with the flap fixed at position 1 is presented in figure 9 for an edge velocity $U_e = 11.75$ cm s^{-1}. This corresponds to a Reynolds number based on the length of the model equal to 1.5×10^4. From this information, the pressure gradient distribution in the ξ-direction was derived via $\mathrm{d}p/\mathrm{d}\xi = -U_e\ \mathrm{d}U_e/\mathrm{d}\xi$ and the distribution of the pressure coefficient, C_f was calculated (Mezaris 1979). It is known that at a short distance beyond the point of flow reversal on the wall the pressure and outer flow velocity level off (Smith 1986). This region was reached at about $\xi = 90$, which is beyond the data reported in figure 9.

The mean velocity of the outer oscillatory flow at the edge of the boundary layer as well as the amplitude of oscillation for frequencies $f_d = 0.2$ and 0.5 Hz are also shown in figure 9. Note that in both cases, the amplitude of oscillation is actually decreasing with downstream distance. The extreme positions of the flap for these two frequencies were actually a little different. Visualization of the steady flow for the two extreme flap positions and flap arrangement for $f_d = 0.2$ and 0.5 Hz have been included in Mezaris & Telionis (1980). Here we display in figure 10, plate 1, the visualization for $f_d = 0.2$ Hz.

A very interesting feature of steady flow reversal is apparent in this figure. The location of

flow reversal is visually estimated for figure 10(II) at $\xi = 36$ mm. There follows a region approximately 38 mm long, of almost stagnant flow. This separated region is extremely thin and generates very small disturbances in the outer flow. Further downstream, a more violent interaction with the outer flow is evident. Very similar patterns are apparent in the frames included in Mezaris & Telionis (1980) for $f_d = 0.5$ Hz.

Measured velocity profiles for steady flow and flap position I are shown in figures 11 and 12. The profile of zero-wall shear must be a little upstream of station $\xi = 40.64$ mm, because at this station, reversing flow already exists. For flap position II, the station $\xi = 61$ mm must be very near the location of zero wall shear as shown in figure 13. The location of flow reversal as determined by the visual method and the LDV data is in good agreement.

11

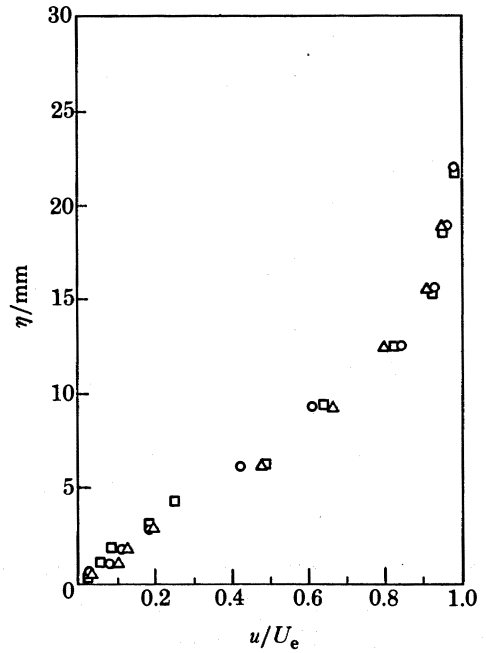

12

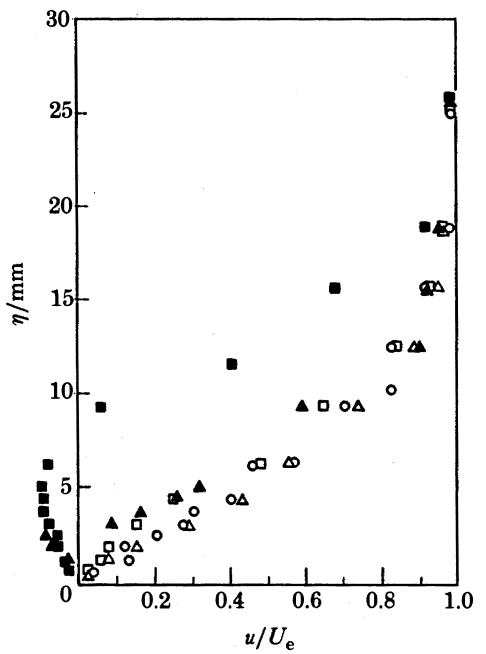

FIGURE 11. The velocity profile for steady flow, and flap position 1. Symbols: ○, $\xi = -61$; △, $\xi = -30.5$; □, $\xi = -15.25$.

FIGURE 12. The velocity profile for steady flow and flap position 1. Symbols: △, $\xi = 0$; ○, $\xi = 11.6$; ▲, $\xi = 40.64$; ■, $\xi = 63.5$.

Even for steady outer flow the phenomena under consideration are inherently unsteady. This becomes obvious by observing a sequence of flow visualization frames obtained with an outer flow speed of $U_e = 8$ cm s^{-1} (figure 14, plate 2). The dye is emitted a little upstream of the origin of the coordinate system and therefore allows visualization of the free shear layer.

To reveal the natural frequency in the free shear layer, measurements were obtained at stations 1, 2 and 3 (figure 8) and at different elevations. Figure 15 shows typical frequency spectra at two points of station 2. The LDV is located in the outer flow and picks up a clean peak at the natural frequency. The HF is situated within the wake and shows a few more frequencies that are not related to the natural frequency. In many cases the first and the second harmonic can also be detected. The spectra indicate clear peaks at station 2 where, approximately, streaklines develop the first roll-up as shown in the flow visualization of figure 14.

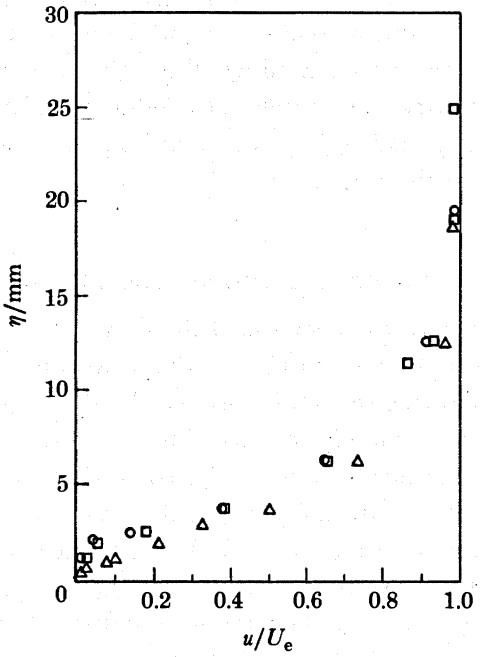

FIGURE 13. The velocity profile for steady flow and flap position II. Symbols: △, $\xi = 50.8$; □, $\xi = 55.9$; ○, $\xi = 61$.

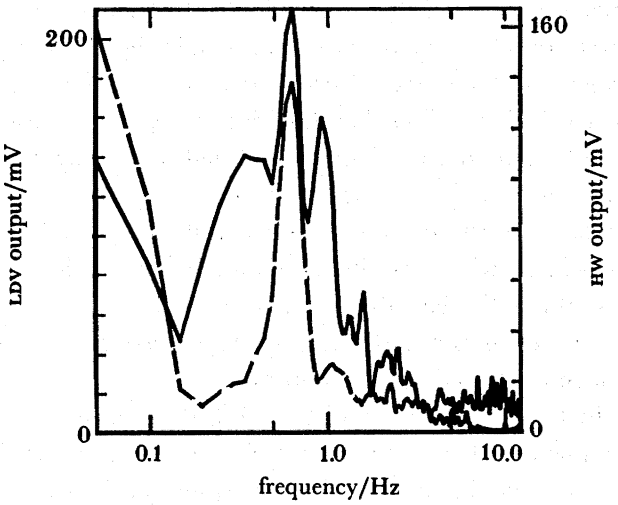

FIGURE 15. Frequency spectra of the velocity for undisturbed flow at $x = 15$ cm. – – –, LDV at $y = 1.4$ cm; ——, HF at $y = -1.1$ cm.

From all the data obtained at $U_e = 8$ cm s^{-1}, the natural frequency of the phenomenon appears to be approximately 0.58 Hz, but frequencies between 0.45 and 0.70 Hz were not unusual. Ho & Huang (1981) note that their mixing layer developing between two water streams of 9.0 and 5.0 cm s^{-1} respectively indicated vortices in a non-periodic manner, but their spectrum displayed a peak at a frequency close to the theoretically determined 'most amplified' frequency (Monkewitz & Huerre 1982). The problem under consideration here is certainly quite different, because on one side of the shear layer, the wall provides a significant obstruction.

Rather, we would say that our separating shear layer is a mixing layer that becomes 'progressively free' as it moves downstream. The differences between the two cases are accentuated by the fact that the first instabilities, those that could be modelled by a linear stability theory, develop quite early, and therefore the influence of the wall cannot be ignored. The reduced response frequency, $2\pi f_r \theta/U_\infty$, was found equal to approximately 0.12, where θ is the momentum thickness at the origin.

5. The separating shear layer

This and the next section discuss the response of the flow to periodic disturbances imposed externally. In the present section we concentrate on the separating shear layer, namely region III of figure 1, whereas the following section is concerned with the separating boundary layer and the vortical part of the wake, namely regions I and IV of figure 1.

One of the basic questions that needs to be addressed is whether the natural frequencies of the phenomenon interact with the externally imposed pulsation. However, the definition of 'natural frequency' here is itself a formidable task. For a blunt two-dimensional body, as for example a circular cylinder, the wake organizes itself in the form of large-scale vortices that alternate at the Strouhal frequency f_s. The reduced natural frequency or the 'shedding frequency' for a circular cylinder, $f_s D/U_\infty$, with D the diameter of the cylinder and U_∞ the speed of the approaching stream, is very near to 0.21, for a wide range of subcritical Reynolds numbers. However, the formation of alternate large-scale vortices occurs far from solid boundaries and is rather the result of the interaction of two vortex sheets of opposite sign. In our problem there is only one free shear layer, and single-sign vorticity is shed in the wake. A case closer to the present problem is the free-shear layer that separates two parallel streams of different but uniform velocities. Even for this ideal case, the natural frequency is not any more fixed. Rather, we can talk about a 'most amplified frequency' and a classical statistical distribution of frequencies around it (Michalke 1972).

The separated shear layer of the present problem rolls up as shown in figure 14. There is a natural frequency associated with this phenomenon. In this section we discuss the results of measurements basically along the coordinates x, y, namely, along the free shear layer and downstream of separation. This is essentially a study of natural frequencies and a range of driven frequencies and their harmonics and subharmonics.

The data discussed in this section were obtained with a tunnel speed of 8 cm s^{-1}, unless otherwise stated. The mean velocity profile at $\xi = 0$ was measured repeatedly and the displacement thickness was calculated from the experimental data to be $\delta^* = 0.569$ cm. The temperature was controlled and kept always at 23.5 °C. These conditions correspond to the following Reynolds numbers based on the displacement thickness and the momentum thickness, respectively

$$Re_\delta = U_\infty \delta^*/\nu = 492; \quad Re_\theta = U_\infty \theta/\nu = 234. \tag{1}$$

At this speed the natural frequency of the rolling up in the separated shear layer was found to be 0.58 Hz.

The frequency of the external disturbance was varied from 0.2 to 0.7 Hz in increments of 0.1, including the subharmonic of the natural and extending well above the natural frequency. Data were taken at three points at each of the stations 1, 2 and 3 shown in figure 8. Then,

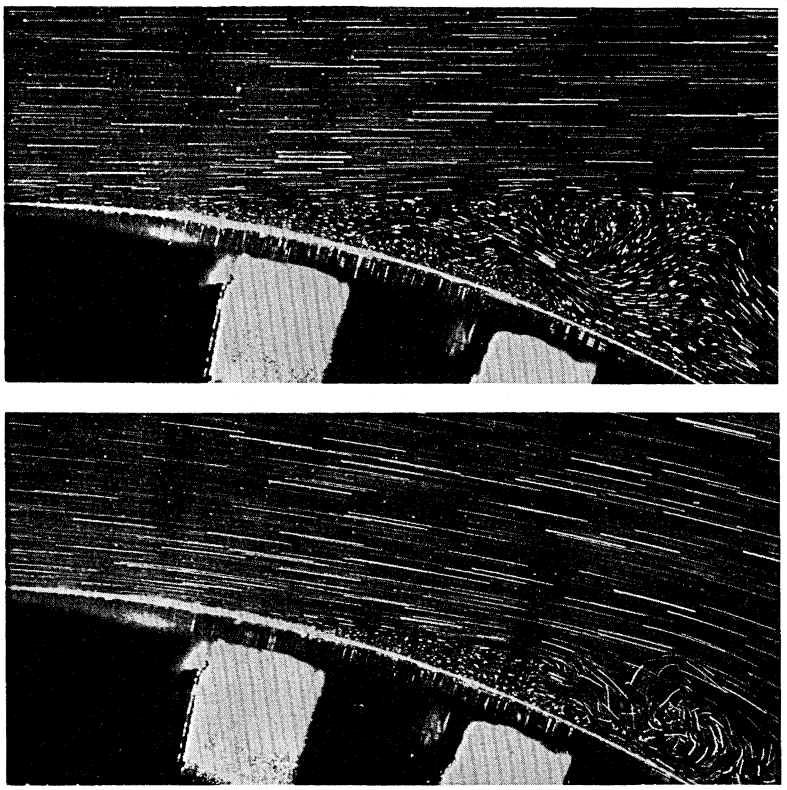

FIGURE 10. Flow visualization for extreme positions of the flap. Steady case with flap arrangement corresponding to $f_d = 0.2$ Hz. Top: position I; bottom: position II.

(*Facing p.* 508)

PHILOSOPHICAL TRANSACTIONS OF THE ROYAL SOCIETY A MATHEMATICAL, PHYSICAL & ENGINEERING SCIENCES

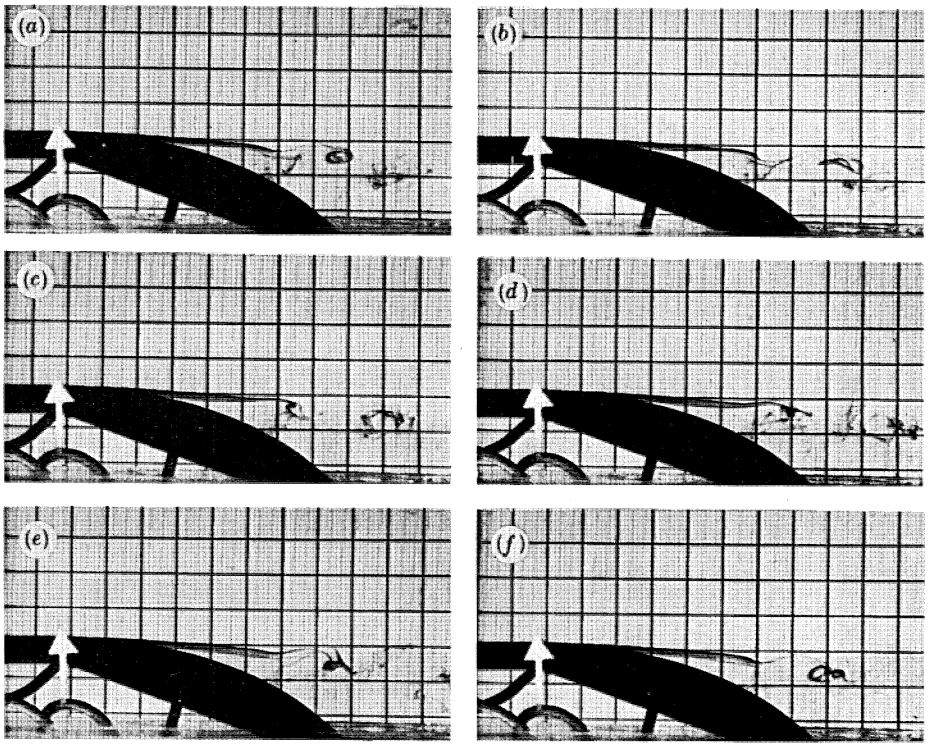

FIGURE 14. Dye-flow visualization for undisturbed flow at $U_\infty = 8$ cm s^{-1}. (*a*) $t = 0.0$; (*b*) $t = 0.43$; (*c*) $t = 0.86$; (*d*) $t = 1.29$; (*e*) $t = 1.72$; (*f*) $t = 2.15$.

PHILOSOPHICAL TRANSACTIONS OF THE ROYAL SOCIETY A MATHEMATICAL, PHYSICAL & ENGINEERING SCIENCES

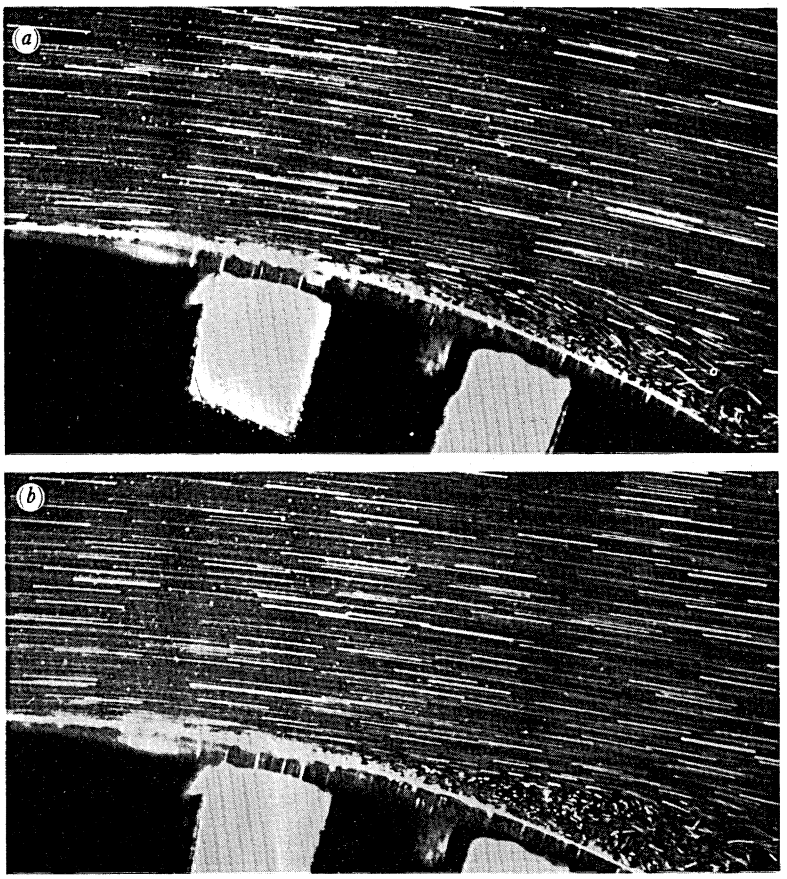

FIGURE 18*a*, *b*. Flow visualization of small intervals within one period, T, for $f_d = 0.2$ Hz. (*a*) $t = 0$; (*b*) $t = \frac{1}{10}T$.

PHILOSOPHICAL TRANSACTIONS OF THE ROYAL SOCIETY A MATHEMATICAL, PHYSICAL & ENGINEERING SCIENCES

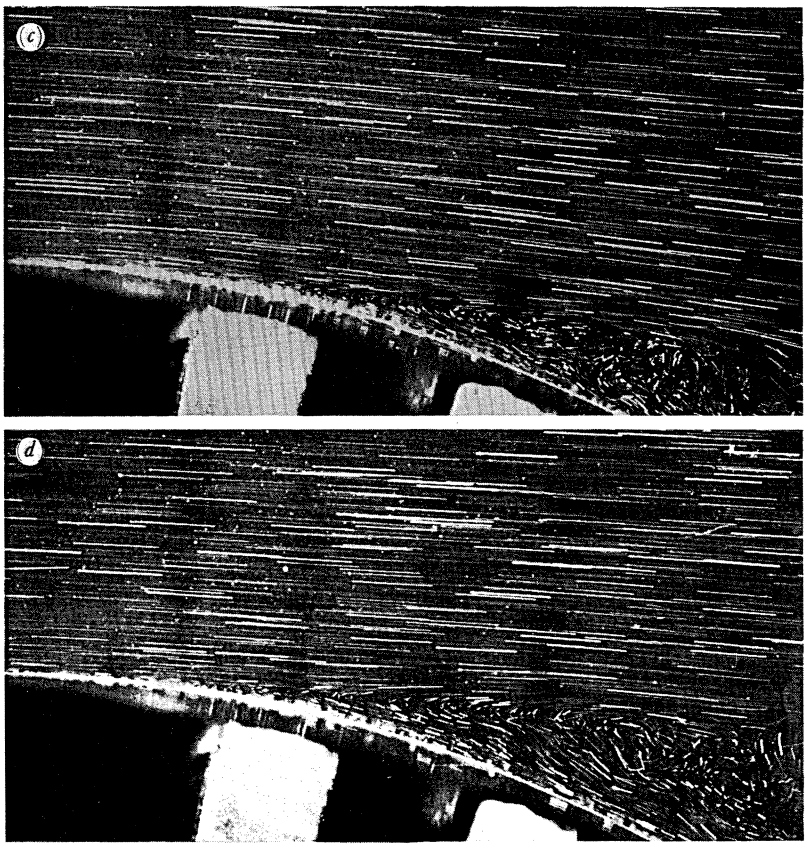

FIGURE 18*c*, *d*. Flow visualization of small intervals within one period, T, for $f_d = 0.2$ Hz. (*c*) $t = \frac{2}{10}T$; (*d*) $t = \frac{3}{10}T$.

PHILOSOPHICAL TRANSACTIONS OF THE ROYAL SOCIETY A MATHEMATICAL, PHYSICAL & ENGINEERING SCIENCES

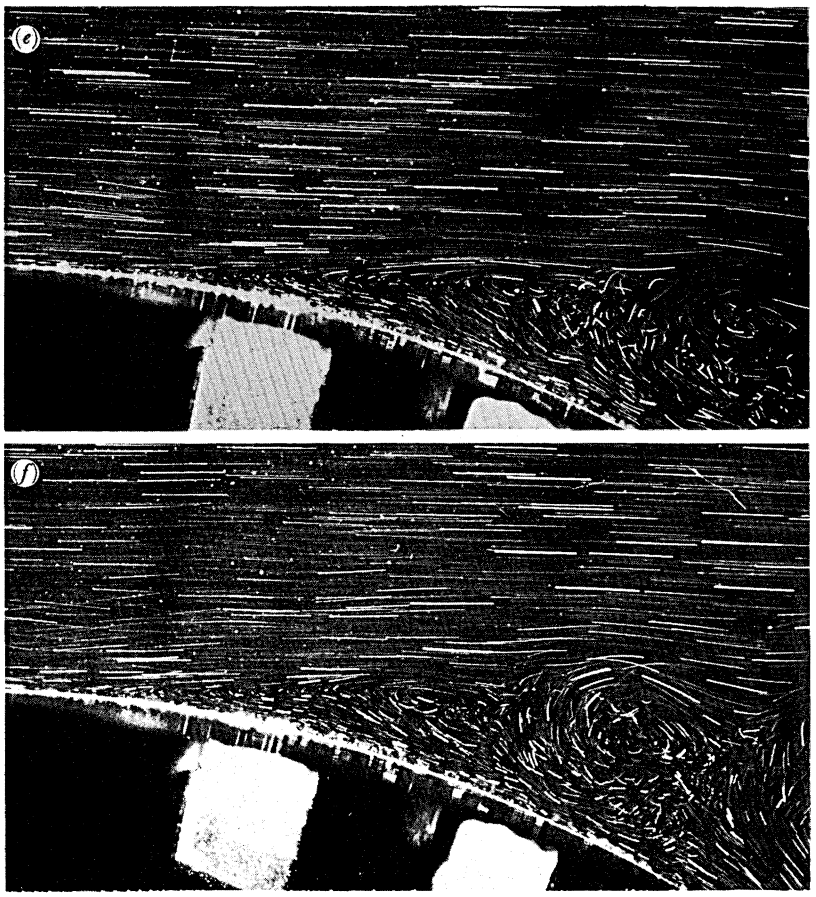

FIGURE 18*e*,*f*. Flow visualization of small intervals within one period, T, for $f_d = 0.2$ Hz. (*e*) $t = \frac{4}{10}T$; (*f*) $t = \frac{5}{10}T$.

PHILOSOPHICAL TRANSACTIONS OF THE ROYAL SOCIETY A MATHEMATICAL, PHYSICAL & ENGINEERING SCIENCES

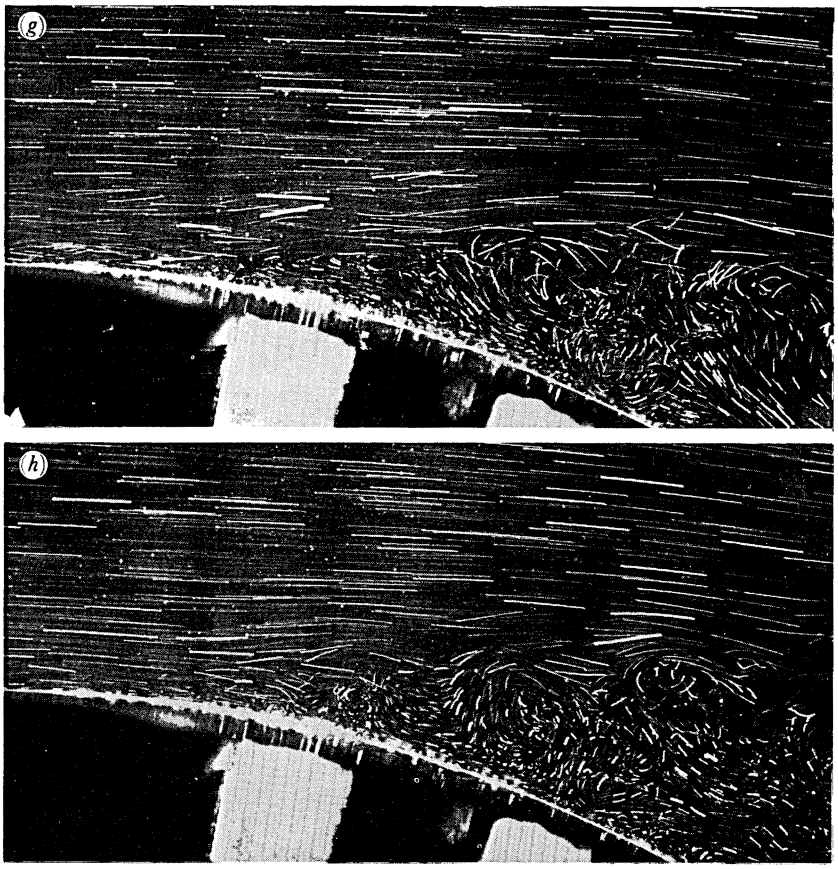

FIGURE 18*g*, *h*. Flow visualization of small intervals within one period, T, for $f_d = 0.2$ Hz. (*g*) $t = \frac{6}{10}T$; (*h*) $t = \frac{7}{10}T$.

PHILOSOPHICAL TRANSACTIONS OF THE ROYAL SOCIETY A MATHEMATICAL, PHYSICAL & ENGINEERING SCIENCES

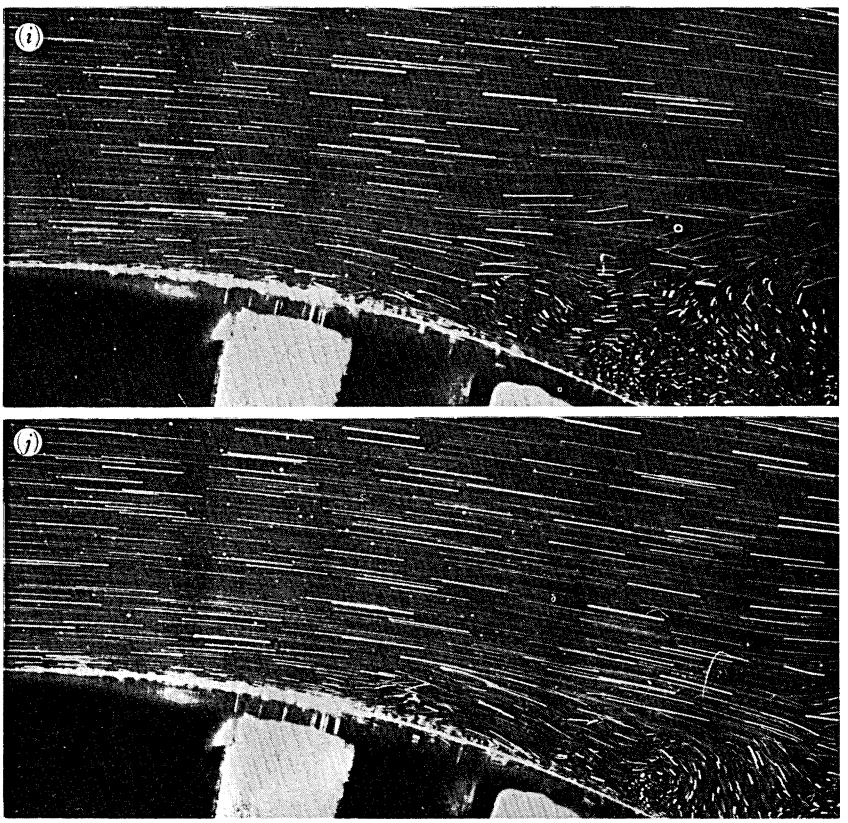

FIGURE 18*i,j*. Flow visualization of small intervals within one period, T, for $f_d = 0.2$ Hz. (*i*) $t = \frac{8}{10}T$; (*j*) $t = \frac{9}{10}T$.

PHILOSOPHICAL TRANSACTIONS OF THE ROYAL SOCIETY A MATHEMATICAL, PHYSICAL & ENGINEERING SCIENCES

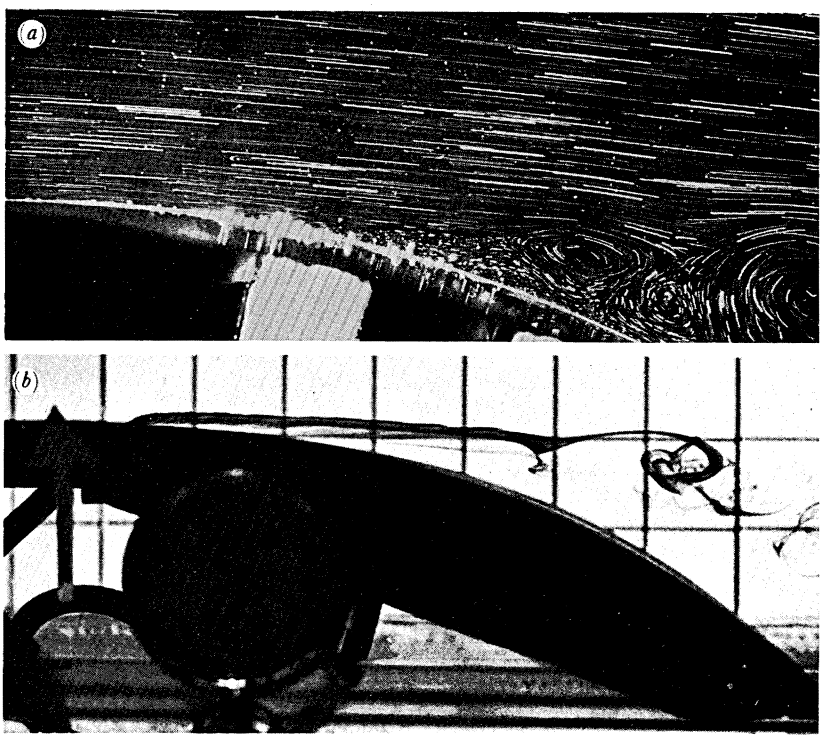

FIGURE 33. Comparison of (*a*) streamlines and (*b*) streaklines.

PHILOSOPHICAL TRANSACTIONS OF THE ROYAL SOCIETY A MATHEMATICAL, PHYSICAL & ENGINEERING SCIENCES

for a driving frequency very close to the natural frequency, namely for $f_d = 0.5$, two profiles were obtained at $x = 2$ and 7 cm, scanning carefully the vertical direction.

Typical data in the frequency domain obtained with the LDV at $x = 10$ cm and $y = -1.1$ cm are shown in figure 16 for a driving frequency equal to $f_d = 0.3$ Hz. In this figure the second harmonic is shown to have a larger magnitude. Considering the fact that the driving frequency is approximately half the natural frequency, we can identify here the phenomenon of subharmonic resonance. Ho & Huang (1981) observed and describe a similar phenomenon, and in fact achieve an increase in the mixing of two streams by driving them at the subharmonic of the natural frequency. Our conclusion is actually subject to criticism (C.-M. Ho, personal communication). The amplifications of the second and third harmonics observed were based on three single point measurements across the shear layer. The eigenfunctions of such instabilities can have strange shapes and therefore may show very large amplitudes at specific points. A more appropriate approach would be to integrate the energy content of a specific frequency across the free shear layer.

The dominant peaks in figure 16 correspond, in ascending order; to frequencies of 0.3, 0.6, 1.2, 1.6 and 2 Hz, respectively. Nonlinear interaction is thus evident in the sense discussed by Miksad and his co-workers (Miksad *et al.* 1982, 1983) as displayed by the appearances of sums of the first two dominant frequencies and their harmonics.

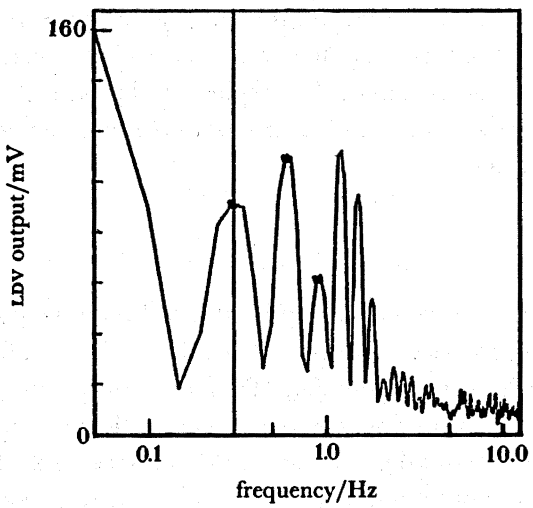

FIGURE 16. Frequency spectrum at $x = 10$ cm, $y = -1.1$ cm for $f_d = 0.3$ Hz.

In the present case, subharmonic resonance is not appearing universally in all the data obtained. It seems that the effect is more clearly identified in the core of the free shear layer rather than the edges. However, a more general trend seems to be persistent: the second harmonic of a driving frequency not necessarily related to the natural frequency or, quite often, the third harmonic are greatly amplified. There seems to be a range of frequencies within which this phenomenon occurs, but our data are not sufficient to pinpoint it.

Spectra of signals obtained at point $x = 10$ cm, $y = 3.5$ cm but for a range of driving frequencies is shown in figure 17. The vertical scale is meaningless because the machine re-adjusts the ordinate to bring the maximum of each curve at the top of the figure. However,

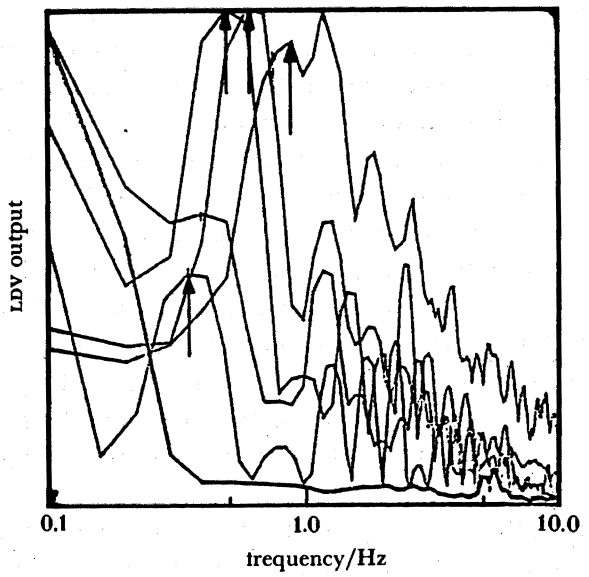

FIGURE 17. Spectra of signals at $x = 10$ cm, $y = 3.5$ cm and driving frequencies $f_d = 0.3$, 0.4, 0.5, 0.6 and 0.8 Hz.

after careful inspection, some very interesting information is revealed. For driving frequencies (marked with an arrow) above the subharmonic of the natural frequency, namely for frequencies larger than 0.3 Hz, the first harmonic of the natural frequency is always amplified, namely 1.2 Hz. This phenomenon cannot be explained by the theory of subharmonic resonance, because now the second harmonic of the natural frequency is excited regardless of the value of the driving frequency.

6. THE WAKE

This section is concerned with the response of the attached boundary layer and the vortical wake, namely regions I and IV, to external disturbances. Averaged and first-harmonic velocity profiles were measured along the coordinates ξ, η. To avoid interpreting the negative lobes of the signal as a higher frequency, averaging was performed in the time domain. A careful and detailed study of the attached boundary layer, flow reversal and the wake region was undertaken. Measurements were obtained at each station by traversing in the y-direction all the way across the separated shear layer. For the results presented in this section, the flow was forced at two frequencies, $f_d = 0.2$ and 0.5 Hz and the tests were performed at a speed $U_e = 11.75$ cm s^{-1}, corresponding to a shear layer natural frequency of 0.85 Hz. Considering as characteristic velocity the mean velocity in the region of the zero-pressure gradient, and as a characteristic length the length of the model, $L = 1.223$ m, reduced frequencies corresponding to the two driving frequencies are $k = 1.97$ and 4.93, respectively. These reduced frequencies should not be compared with reduced frequencies based on the length of a fully submerged model as, for example, the chord length of an airfoil. The Reynolds number based again on the length of the model was $Re = 1.5 \times 10^4$.

A series of flow visualizations corresponding to one cycle of oscillation with frequency $f_d = 0.2$ Hz is presented first in figure 18, plates 3–7. For $t = 0$, the velocities in the entire flow field, even in the wake, are directed downstream. No flow reversal can be observed. In other

words, particles that were part of the wake and were moving slowly upstream, are now realigned with the flow. A region of random motion near the wall initiates at $\xi = 68$ mm but this is the history, or more descriptively, the 'remnants' of the randomness in the wake. In other words, frozen patterns of vortices are swept away uniformly in the main direction of the outer flow. At $t = \frac{1}{10}T$, with T the period of the disturbance, the outer flow decelerates and reverse flow can be clearly seen. The point of zero skin friction moves upstream until the time $t = \frac{5}{10}T$ when it reaches its extreme upstream position at $\xi = 15.4$ mm. After this instant, the point of zero skin friction changes direction and starts moving downstream, whereas the wake continues to grow in thickness.

It has been argued (Despard & Miller 1971; Koromilas & Telionis 1980) that for oscillatory flow, the position of separation is displaced with respect to its quasisteady position but remains unaffected by the oscillations of the outer stream. Although not far from this idealized condition, the visualizations of figure 18 do not indicate exactly this behaviour. We may assume that the position of separation is somewhere in the region 50 mm $< \xi <$ 65 mm. For $t < \frac{5}{10}T$, the point of zero skin friction shoots way upstream of this neighbourhood. However, after $t = \frac{5}{10}T$ the wake gathers strong large-scale vortices that push the outer bounds into the region of potential flow. For $t = \frac{8}{10}T$ and $t = \frac{9}{10}T$ the average momentum in the wake and its thickness reduce significantly. The position where the outer flow decisively leaves the boundary is then approximately near $\xi = 65$ mm.

Although the flow visualizations may contain some flow patterns like the ones suggested by Moore (1957); Rott (1956); Sears (1956); Sears & Telionis (1975) that may signal the onset of separation, it is rather difficult to identify them. Such identification would require moving the frame of reference with the speed of separation. What can be said with certainty is that in most frames, the region of large-scale wake turbulence is separated from the point of zero skin friction by a region of very slow and well-ordered flow, which may be partly reversed in direction.

Next, we turn our attention to the LDV measurements and the profiles of mean velocity and their amplitudes. The raw data are plotted separately in the figures that follow. Unfortunately, some points are very crowded, especially in the neighbourhood of the origin. Detailed graphs at each station, in the form originally produced by the computer, are included in Mezaris (1979). To avoid overcomplicating these figures, curves were obtained and plotted separately. In figure 19, for example, the actual data points for the averaged velocity profiles are shown for $f_d = 0.2$ Hz and the corresponding computed curves are plotted in figure 20. The profile of the mean velocity at station $\xi = 50$ mm has zero slope at $\eta = 0$, i.e. the skin friction vanishes there but the flow visualizations do not indicate any abrupt change of the flow at this station. The amplitudes of the oscillatory motion in the boundary layer exhibit an interesting behaviour as shown in figures 21 and 22. At $\xi = -61$ mm, the amplitude has the value zero at $\eta = 0$, attains a maximum greater than 1 at $\eta = 1.5$ mm and approaches 1 at approximately $\eta = 6.4$ mm. The same behaviour is exhibited by the amplitudes at subsequent ξ-stations. This behaviour has been quite familiar to investigators and it has been predicted by analytical calculations as discussed in review articles (Telionis 1979, 1980, 1981).

As we move further into the area of increasing adverse pressure gradient, the maximum amplitude increases sharply and the oscillatory layer extends further into the flow. This behaviour continues until $\xi = 55.9$ mm, where the peak near the wall takes the value 14 and the profile approaches the value 1 at a distance from the wall equal to the thickness of the

PHILOSOPHICAL TRANSACTIONS OF THE ROYAL SOCIETY A MATHEMATICAL, PHYSICAL & ENGINEERING SCIENCES

19

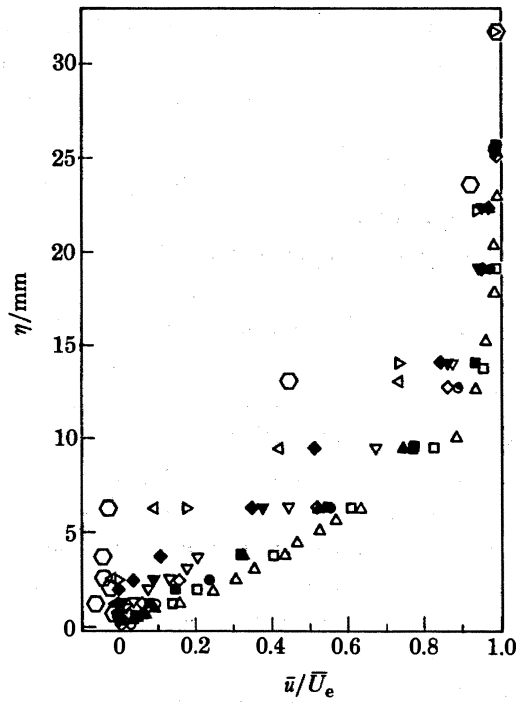

20

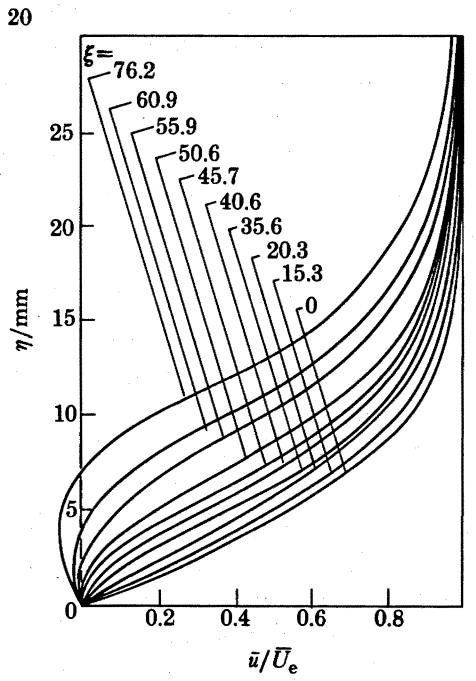

FIGURE 19. Mean velocity profiles for $f_d = 0.2$ Hz and different ξ stations: ○, −61; △, 0; □, 15.3; ▲, 20.3; ●, 25.4; ■, 30.5; ◇, 35.6; ▽, 40.6; ▼, 45.3; ◆, 50.8; ▷, 55.7; ◁, 60.9; ○, 76.7.

FIGURE 20. Velocity profiles derived from figure 19 by curve fitting.

21

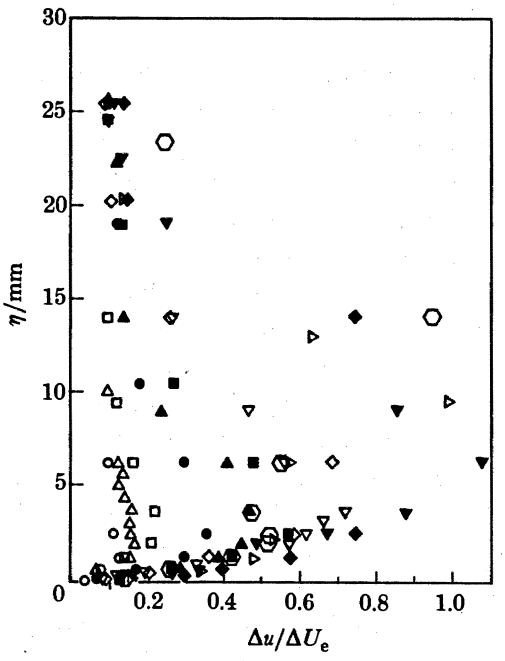

22

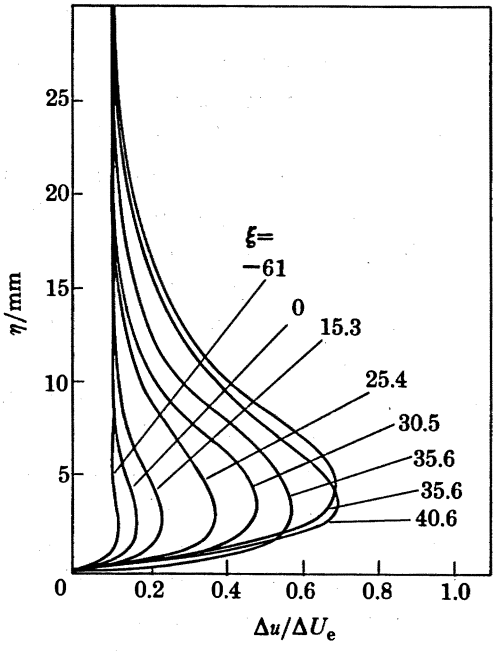

FIGURE 21. Reduced amplitude of the velocity for $f = 0.2$ Hz at different ξ stations. Symbols: ○, −61; △, 0; □, 15.3; ●, 25.4; ▲, 30.5; ■, 35.6; ▽, 40.6; ◇, 45.7; ▼, 50.9; ◆, 55.7; ▷, 60.9; ○, 76.2.

FIGURE 22. Velocity profiles derived from figure 21 by curve fitting.

boundary layer at that station. At the next two stations, the amplitudes start decreasing. They display a flat portion in the region where the amplitudes of the earlier stations have their peak and attain a maximum far away from the wall before they approach again the value 1. The maximum of the amplitude extreme, $\Delta u/\Delta U_e = 14$, occurs near the extreme downstream position of the zero skin friction point, downstream of which reversed flow exists throughout the cycle. The very fast growth of the amplitude as separation is approached is interpreted here as a characteristic of the separation point.

Very similar behaviour is exhibited in the case of $f_d = 0.5$ Hz. Flow visualizations have been omitted here because of space limitations. Profiles of the mean velocity and the amplitudes are presented in figures 23–25. Characteristic large-scale vortices were clearly shown in the corresponding flow visualizations (Mezaris 1979). The mean velocity profiles in figures 23–25 have a vanishing wall shear between $\xi = 25.4$ and 30.5, but this is not significant for the overall behaviour of the flow. More interesting are the plots of the amplitudes of oscillation (figures 26 and 27). As predicted by the theory, the thickness of the oscillatory parts of the flow is now smaller. The trend of course is the same and the peak increases sharply for larger ξs until it changes behaviour and starts decreasing after $\xi = 35.6$. It should be emphasized that for both the frequencies tested, the outer part of the amplitude profile continues growing even beyond the point where the peak starts decreasing.

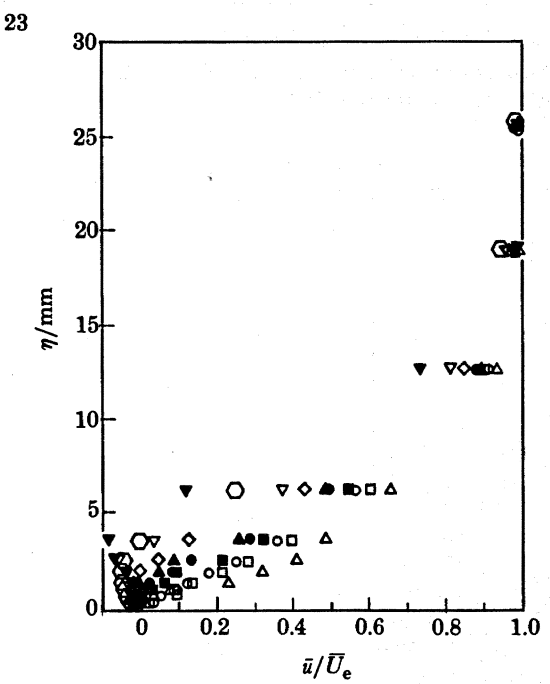

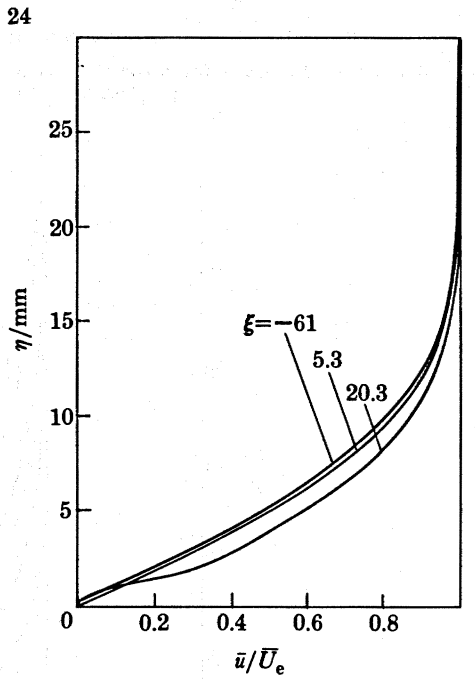

FIGURE 23. Mean velocity profiles for $f = 0.5$ Hz and different ξ stations: ○, −61; □, 15.3; △, 20.3; ■, 25.4; ●, 30.5; ▲, 35.6; ◇, 40.6; ▽, 45.7; ○, 50.8; ▼, 55.8.

FIGURE 24. Velocity profiles derived from figure 23 by curve fitting ($\xi = -61$, 5.3, 20.3).

To expose more clearly the behaviour described above, constant amplitude contours were prepared and are displayed in figures 28 and 29. What seems to be intriguing is the fact that in both cases, a distinct peak can be identified. For the two frequencies investigated here, it appears that the peak is closer to the wall for the higher frequencies. As indicated in the earlier

25

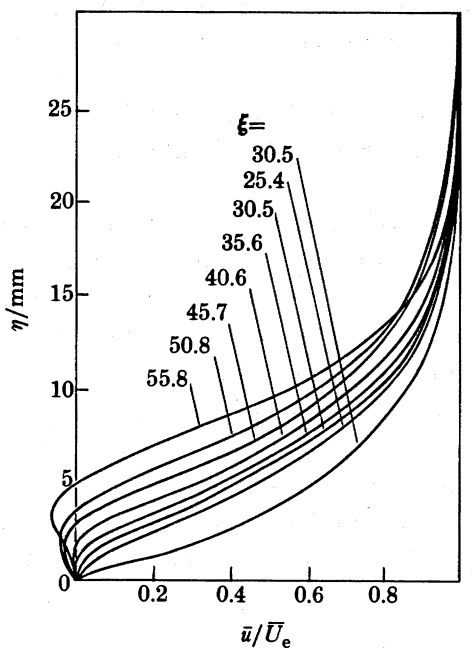

26

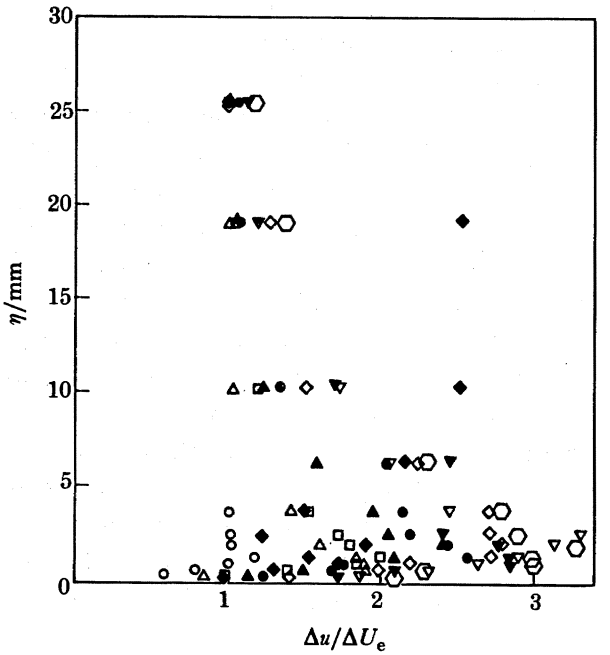

FIGURE 25. Velocity profiles derived from figure 23 by curve fitting ($\xi = 30.5$–55.8).

FIGURE 26. Reduced amplitudes of the velocity for $f_d = 0.5$ Hz at different ξ stations: ○, −61; △, 15.3; □, 20.3; ▲, 25.4; ●, 30.5; ▽, 35.6; ◇, 40.6; ▼, 45.7; ○, 50.8; ◆, 55.9.

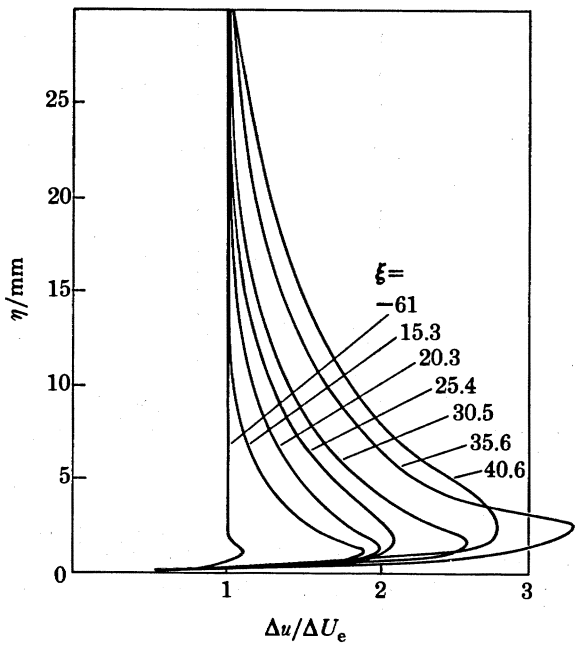

FIGURE 27. Velocity profiles derived from figure 26 by curve fitting.

PHILOSOPHICAL TRANSACTIONS OF THE ROYAL SOCIETY A MATHEMATICAL, PHYSICAL & ENGINEERING SCIENCES

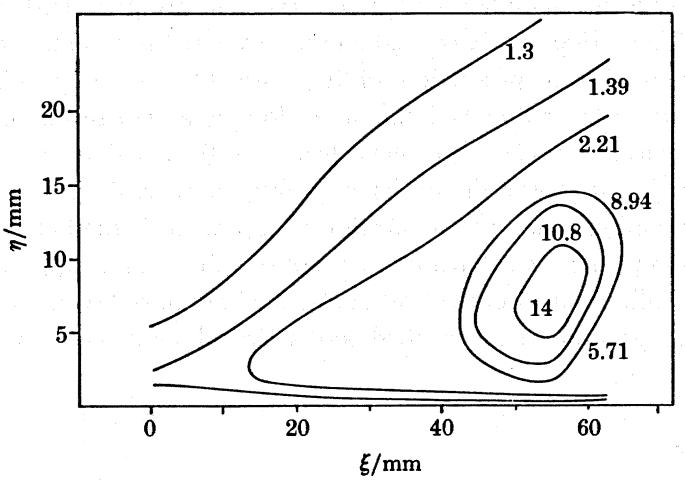

FIGURE 28. Contours of constant amplitude of the velocity fluctuations for $f_d = 0.2$ Hz.

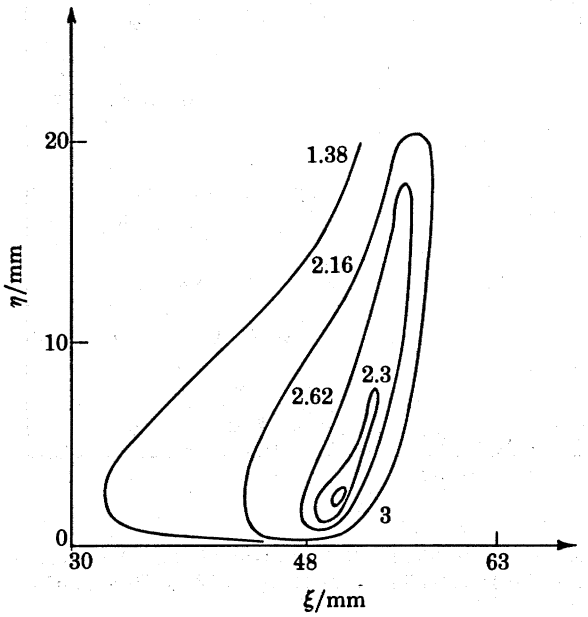

FIGURE 29. Contours of constant amplitude of the velocity fluctuation for $f_d = 0.5$ Hz.

figures as well, immediately next to the wall, the variation of the amplitude is very sharp. Moreover and more importantly, the peak is located approximately at $\xi = 55$ and 50 mm for $f_d = 0.2$ and 0.5 Hz, respectively. Therefore the peak moves upstream for higher frequencies. It should be emphasized that the data obtained with LDV cover a region well within the separated flow; this is a necessary condition for capturing the amplitude peak.

Investigating turbulent separating flows, Simpson (1977) and Kenison (1977) reported that the r.m.s. of the random fluctuations grow sharply as separation is approached. The trend is of course the same, and the analogy between the amplitude of random oscillations and organized driven oscillations is obvious. In fact, Kenison plotted a set of contours very similar to those shown in figures 28 and 29. However, because of lack of data, Kenison's curves terminate exactly at the peak, namely at separation, and do not close downstream.

Phase differences were also calculated for $f_d = 0.2$ Hz, and are presented in figure 30. For the very early stages of flow, that is at $\xi = -60.96$ mm, over the flat portion of the plate, the behaviour is in agreement with the predictions of the classical theory (Lighthill 1954; Telionis 1979, 1981). The boundary-layer flow lags the outer flow by a very small phase angle. Very near the wall, the behaviour is reversed; a phase lead is indicated that seems to tend to 45° at the wall, a value predicted by the theory for high-frequency oscillations (Lighthill 1954). At subsequent stations, and especially as separation is approached, the behaviour is not very clear. The basic trends appear to be: sharp increases of the phase angle approaching values of up to 130° next to the wall, uniform phase lead across the boundary layer, continuous growth of the phase advance as separation is approached, and a central region with almost no variation of the phase.

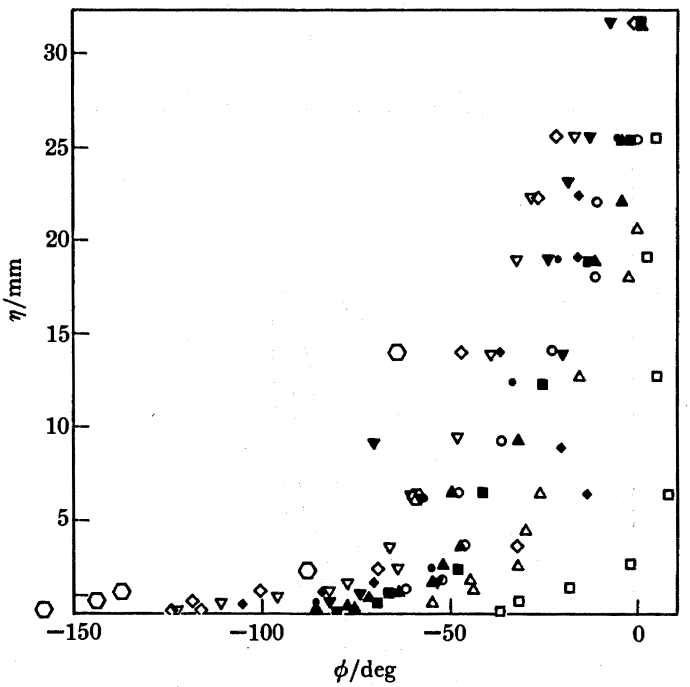

FIGURE 30. Phase angles of the velocity profile, $f = 0.2$ Hz. Symbols: □, −60.96; △, 0.00; ○, 15.25; ▲, 20.32; ■, 25.4; ▼, 30.4; ●, 35.56; ▽, 40.64; ◇, 45.72; ◆, 50.8; ○, 55.88.

The phase plots of figure 30 were obtained by manipulating the averaged time records of the velocity fluctuations. They all indicate a very characteristic and unexpected behaviour. The phase increases sharply from its wall value but not monotonically. At a small distance from the wall, approximately 4 mm, it reverses direction and decreases for a while. To verify this behaviour of the phase, data were obtained again at a different speed ($U_e = 8$ cm s^{-1}) and with a direct method for calculating the phase by the Zonic analyser. The second set of results, obtained about one year later, are plotted in figure 31 for three stations upstream of separation and for a driving frequency of $f_d = 0.35$ Hz. The qualitative trend is identical to that of figure 30.

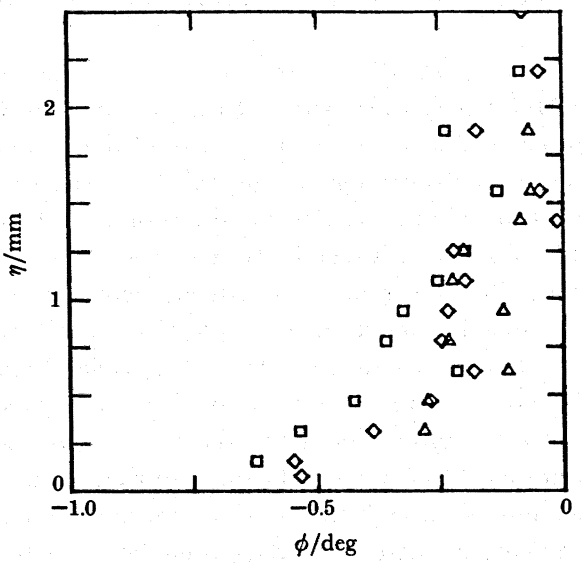

FIGURE 31. Phase profiles at the stations of figure 14 for $f_d = 0.35$ Hz. Symbols: △, $\xi = 6.3$; □, $\xi = 7.5$; ◇, $\xi = 9.5$.

7. Discussion

The present work is concerned with separation of an oscillatory laminar boundary layer. The problem is very complex and at the present our understanding of the phenomenon is rather poor. At the time we initiated this study of unsteady separating flows, we realized that the steady problem had never been studied adequately. In the past two decades, steady separation has received considerable attention by theoreticians (Brown & Stewartson 1969; Stewartson 1974; Williams 1977; Messiter 1983; Smith 1986) but, with the exception of the work of Varty & Currie (1984), most earlier experimental contributions were confined to very low Reynolds numbers. Nevertheless, such results were appropriate for comparisons with analytical theories (Smith 1977). Velocity profiles near steady separation were obtained by Varty & Currie (1984) and Mezaris & Telionis (1980). A comparison of some of Varty & Currie's steady separation data with analytical results appears in Smith (1986).

It has been argued and now is accepted widely that, for unsteady flow, the point of zero skin friction is not related to separation. The present evidence indicates that the same may be true for steady flow as well. In other words, there is no qualitative difference between steady or unsteady flow. The point of zero skin friction in both cases initiates a region of thin, reversed but extremely slow-moving flow. Particles in this region appear in the flow visualizations to be motionless. Above this region there seems to be very little disturbance on the outer portion of the boundary layer. Moreover, no randomness is introduced, even at Reynolds numbers of the order of 10^5. Further downstream, some vortical activity becomes evident. The initiation of a violent departure from laminar attached flow surely deserves to be called separation. This, rather than the point of zero wall shear, is where the flow breaks away from the wall. The distance between the point of zero skin friction and the point of separation is very small for steady flow. In the present experiments it is less than one boundary-layer thickness. In a less careful experiment, or in case the overall picture of the flow about an airfoil is needed, it is

conceivable that the points of zero skin friction and separation may not be distinguished in steady flow.

The above discussion is inspired by earlier observations and measurements on airfoils (Carr *et al.* 1977; Telionis 1979; McCroskey 1981, 1982). In wind-tunnel unsteady-flow testings, it was found that a very thin layer of a tracer at the bottom of the boundary layer may shoot fast upstream, without apparently disturbing the outer flow. Separation as we define it here is then detected by an abrupt turning into the flow and responds to the unsteady disturbance at a much smaller pace. This discussion is seemingly contrary to recent theoretical advances (Messiter 1983; Smith 1986). But this is not true. All mathematical theories that match a triple-deck analysis with an inviscid model, for example Kirchhoff's free-streamline theory, predict that quantities like the thickness of the shear layer, the displacement thickness, the angle of the separation line, display no sharp variations near flow reversal and tend to zero for $Re \to \infty$, with some inverse power of the Reynolds number. This is in agreement with steady-flow experimental findings in the sense that no significant disturbance in the variation of such quantities is observed as one moves through the point of zero skin friction. For some transient impulsive flows, the experiments indicate large deviations between the points of zero skin friction and separation, and this problem has not yet been attacked analytically.

But then, where is the abrupt change that some experimentalists have identified as separation? The recent mathematical models predict that downstream of the point of zero wall shear, the flow indeed turns away from the wall. In fact, for subsonic flow, the curvature of the separation line is positive, namely concave upwards (Smith 1986). This behaviour could appear experimentally as an abrupt change of the slope. Our experimental data on the locus of $u = 0$ and the streamline that emanates from the point of zero skin friction are plotted in figure 32. These data represent the average of the pulsating flow field. Indeed, it appears that there is a tendency for positive curvature, in agreement with the predictions of Smith (1986).

But in real life, there is one more significant feature of the flow that is missing from the mathematical models. A few recirculating but active bubbles are trapped a little further downstream from the point of flow reversal, as shown clearly in the flow visualizations of the present paper. Such bubbles have been observed by many other researchers but the most

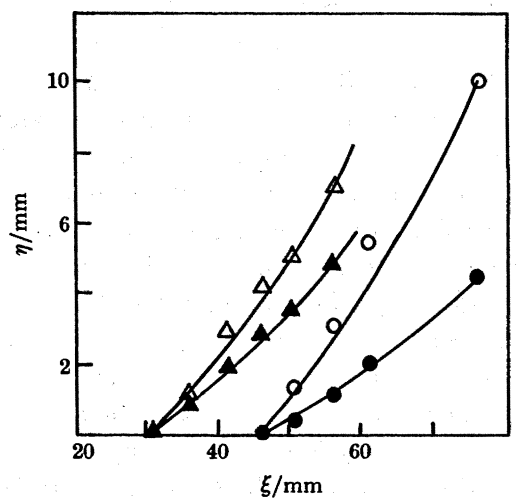

FIGURE 32. Streamlines and zero u-velocity lines emanating from the mean position of zero skin friction.

beautiful visualizations of an unsteady separation were reported by Bouard & Coutanceau (1980). It is our contention here that the presence of such bubbles controls the fate of the ensuing free shear layer, with significant influence on the development of the wake and the pressure distribution over the body. It is then possible that, as $Re \to \infty$, the flow there turns into the stream with a finite angle with respect to the surface of the body. This is the point we call separation. In the terminology of Prandtl (1904), 'a fluidsheet projects itself into the free flow and effects a complete alteration of the motion'. A question then arises: are these bubbles the result of the growth of instabilities of the free shear layers or are they the response of the flow to the global characteristics of the separated region? We believe that the second is true, and we will argue this point later, in relation to the interaction of natural and forced periodic disturbances.

When periodic disturbances are imposed on a separated region, the wake may synchronize with the disturbing frequency. The phenomenon has been well known to investigators of flow induced vibrations as 'lock-on' (see, for example, Stansby 1976; McCroskey 1977; Griffin 1981; Barbi *et al.* 1986). The range of driving frequencies for which lock-on occurs is a function of the amplitude of the imposed oscillation. In such studies, however, interest is concentrated on the ranges of frequencies, the amplitudes of forces, and perhaps the coupling with mechanical vibrations. The present study has been essentially a closer look at the free shear layer, the separated region and the wake of a flow driven with frequencies around the natural frequency. Emphasis is therefore given here to the flow properties rather than gross effects like drag and lift.

It has been known that the large-scale vortices shed alternately over a blunt body determine the shedding frequency. The process depends heavily on the interaction of the two shear layers that emanate from the two points of separation. Actually, in this problem there are two different natural frequencies involved: the frequency of vortex shedding and the frequency of the shear layer roll-up. Our earlier experimental data (Barbi *et al.* 1981) for flows over circular cylinders indicate that these two frequencies are independent of each other. Professor C.-M. Ho (personal communication) had earlier arrived at a similar conclusion.

The situation is quite different in the problem considered here, because there is only one shear layer. We should then anticipate again the appearance of two natural frequencies: the most-amplified frequency of the free shear layer and the natural shedding frequency of the wake. Our evidence indicates that the natural frequency we detected is not consistent with the classical results of both theory and experiment on free shear layers (Ho & Huang 1982). But then, the physical situation here is different. In the classical problem, a shear layer is allowed to develop between two streams that are otherwise undisturbed. Instabilities grow but it takes a considerable distance downstream before phenomena like shear-layer roll up, vortex pairing, nonlinear interaction of disturbances, transition and turbulence occur. In the present case, the shear layer develops over, and very near to, a solid surface. This surface allows the presence of a few vortices that are fully developed to be lodged underneath the lifting shear layer, at a distance far shorter than necessary for the growth of natural instabilities. The evidence presented here seems to indicate that for the Reynolds numbers examined, the free shear layer instabilities play a minor role in the development of the wake. What appears as roll-up in dye visualizations is just the response to the growth and drifting of large-scale coherent structures in the wake. This is clearly demonstrated in the two flow visualizations of figure 33, plate 8. The streakline indicates a behaviour reminiscent of the cat's eyes in classical stability results. However, examination of the instantaneous flow field (averaged over $\frac{1}{8}$ s), indicates that the

PHILOSOPHICAL TRANSACTIONS OF THE ROYAL SOCIETY A MATHEMATICAL, PHYSICAL & ENGINEERING SCIENCES

dye shapes simply mark the outer periphery of a set of vortices. The interpretation adopted here then is that the existence of vortices downstream of the point of zero skin friction give rise to an undulating shear layer that imitates the behaviour of an unstable free shear layer.

Smith (1985*b*) points out that four types of natural instabilities can be triggered off near separation. All types are interlinked through the Tollmien–Schlichting type, which can excite Görtler vortices by means of three dimensionality (Hall & Smith 1984), or Kelvin–Helmholtz on a broader scale or even Rayleigh waves on a short or long scale (Bodonyi 1985; Smith & Bodonyi 1985). In his report, Smith (1985*b*) demonstrates that on linear grounds, there is a definite distance downstream of separtion at which abrupt disturbance growth will occur. This distance is given by the formula

$$X_{\text{crit}} = (\Omega/3b^2)^{\frac{1}{3}}, \quad b \simeq 0.44. \tag{2}$$

In recent numerical calculations based on the parallel flow assumption and interacting boundary layers, Nayfeh *et al.* (1986) presented numerical calculations indicating indeed a very fast growth of the amplitude of waves that, however, is almost uniform in a domain that starts a little upstream and extends beyond the point of flow reversal.

There is a significant difference between the flows examined analytically by these authors and the flow investigated here. Our disturbance is introduced into the outer flow. The viscous layer is driven everywhere along its edge. The idea of disturbance growth therefore is not applicable. The response of our viscous layer is not a travelling wave either, because the edges of all points are driven in phase with the inviscid flow. Nevertheless, the concept of a growing disturbance is not altogether foreign to the phenomenon under consideration. This is because as we move downstream we find that the external disturbance amplitude decreases but instead the amplitude of the oscillation increases rapidly. What we have captured here is not any of the well-studied instabilities, and yet it is possible that the growth of our disturbances is controlled by the mechanisms identified by Smith (1985*b*). To compare with this theory, we have calculated the distance ξ_{crit} from (2), rewritten here in the present notation

$$\frac{\xi_{\text{crit}}}{L} Re^{\frac{3}{8}} = \left[Re^{-\frac{1}{4}} \frac{2\pi f l}{U_\infty} \frac{1}{3b^2} \right]^{\frac{1}{3}}. \tag{3}$$

For $\lambda = 1, f = 0.2$ and 0.5 Hz, we found it to be 57 and 77 mm, respectively. These quantities are perhaps larger than the distances between the points of mean flow reversal and the points of maximum amplitude. But the order of magnitude and the trend appear to be consistent.

In the terminology of flow-induced vibrations, we can probably state that the wake in our experiments was always locked on the frequency of the external disturbance. The natural frequency or its harmonics have surfaced in some of the experiments but their magnitude was considerably smaller than the magnitude of the driving frequency, unless resonance was at hand. When the flow was driven at its natural frequency no special effects were observed. However, disturbances of lower frequencies lead to second harmonic growth and a phenomenon reminiscent of subharmonic resonance.

Before we discuss further the properties of the point of separation itself, we should emphasize the difference between the present investigation and the work of Despard & Miller (1971). In the present work, the distribution of the adverse pressure gradient changes periodically, thus simulating more accurately the flow about a pitching airfoil. In Despard & Miller (1971) the approaching flow changes only in magnitude. The present investigation was conducted at

$Re = 1.5 \times 10^4$ whereas Despard & Miller used a Reynolds number larger than 10^5. The reduced frequencies here were $k = 1.97$ and 4.93, whereas Despard & Miller employed a range of 2 Hz $< f <$ 240 Hz and performed tests at reduced frequencies calculated on the length of the model in the range $10 < k < 40$.

One of the controversies between the results of Despard & Miller and those of the present group is centred around the displacement of separation. Despard & Miller (1971) and Koromilas & Telionis (1980) argued that, for oscillatory flow, separation is displaced upstream and downstream respectively, with respect to its quasi-steady position. Unfortunately, the present evidence is inconclusive on this point. In both efforts, a pre-wake region was identified that expanded and contracted with the frequency of the externally imposed disturbance. However, the present evidence is again inconclusive with respect to the validity of the Despard & Miller criterion of separation, namely 'the position at which the skin friction oscillates between zero and some negative value'. More work is under way at VPI and SU, and this criterion is carefully being considered.

A point on which there is agreement between the present work and the work of Despard & Miller is that the instantaneous position of separation is rather insensitive to the periodic disturbances. However, this by no means implies that the wake too is unaffected by the disturbances. On the contrary, our flow visualizations indicate that the organization of the vortical flow in the wake orders itself to predictable and repeatable patterns. Moreover, the dimension of the wake in the direction perpendicular to the wall fluctuates with the same period.

One of the most interesting discoveries of the present investigation is the pattern of the velocity amplitudes; this is most clearly presented in the form of contours. It is felt that the main contribution here is the demonstration of the fact that a lot of valuable information lies downstream of separation and all sensing methods should be extended into this region. Indeed it was proved that constant amplitude contours close around separation and the data clearly indicate the existence of a distinct peak.

The construction of the water tunnel used in this and earlier work on unsteady separating flows was supported by the U.S. Army Research Office (grant no. DAAC04-75-G-0067). Processing of the present data and the writing of the present article were carried out at VPI, during a period when the work of D.P.T. in this area was supported by the U.S. Air Force Office of Scientific Research (grant no. 82-0228). The same author is thankful to Dr Saad Ragab for many clarifying and stimulating discussions on triple-deck theory. The reviewers of this paper have provided very detailed and constructive criticism. Their contribution is gratefully acknowledged.

References

Barbi, C., Favier, D., Maresca, C., Jones, G. S. & Telionis, D. P. 1986 Vortex shedding from a circular cylinder in pulsating flow. *J. Fluid Mech.* **170**, 527–544.

Bodonyi, R. J 1985 In *Proc. Symp. on Stability of Spatially-Varying and Time-Dependent Flows*. NASA Langley Research Centre.

Bouard, R. & Coutanceau, M. 1980 The early stage of development of the wake behind an impulsively started cylinder for $40 < Re < 10^4$. *J. Fluid Mech.* **101**, 583–607.

Browand, F. K. & Weidman, P. P. 1976 Large scales in the developing mixing layer. *J. Fluid Mech.* **76**, 127–144.

Brown, S. N. & Stewartson, K. 1969 Laminar separation. *A. Rev. Fluid Mech.* **1**, 45–72.

Brown, G. L. & Roshko, A. 1974 On density effects in turbulent mixing layers. *J. Fluid Mech.* **74**, 775–816.

Carr, L. W., McAlister, K. W. & McCroskey, W. J. 1977 *Analysis of the development of dynamic stall based on oscillating airfoil experiments*. NASA TN D-8382.

PHILOSOPHICAL TRANSACTIONS OF THE ROYAL SOCIETY A MATHEMATICAL, PHYSICAL & ENGINEERING SCIENCES

Corcos, G. M. & Sherman, F. S. 1976 Vorticity concentration and the dynamics of unstable free shear layers. *J. Fluid Mech.* **73**, 241–264.
Despard, R. A. & Miller, J. A. 1971 Separation of oscillating boundary-layer flows. *J. Fluid Mech.* **47**, 21–31.
Didden, N. & Ho, C.-M. 1985 Unsteady separation in a boundary layer produced by an impinging jet. *J. Fluid Mech.* **160**, 235–256.
Griffin, O. M. 1981 Universal simularity in the wakes of stationary and vibrating bluff structures. *Trans ASME* I **103**, 52–58.
Hall, P. & Smith, F. T. 1984 *Stud. appl. Math.* **70**, 91.
Hill, P. G. & Stenning, A. H. 1960 Laminar boundary layers in oscillatory flow. *Trans ASME* D **82**, 593–608.
Ho, C.-M. & Huang, L. S. 1982 Subharmonics and vortex merging in mixing layers. *J. Fluid Mech.* **119**, 443–473.
Ho, C.-M. & Huerre, P. 1984 Perturbed free shear layers. *A. Rev. Fluid Mech.* **16**, 365–424.
Jones, G. S. 1980 Measurement and visualization of vortex shedding – natural and forced. M.S. thesis, Virginia Polytechnic Institute and State University.
Jones, G. S., Barbi, C. & Telionis, D. P. 1981 Natural and forced vortex shedding. In *Unsteady turbulent shear flows* (ed. R. Michel, J. Cousteix & R. Houdeville), pp. 228–247. Berlin: Springer.
Katz, J. 1981 A discrete method for the non-steady separated flow over an airfoil. *J. Fluid Mech.* **102**, 315–328.
Kenison, R. C. 1977 An experimental study of the effect of oscillatory flow on the separation region in a turbulent boundary layer. In *Unsteady aerodynamics*. AGARD-CP-227, paper no. 20.
Koromilas, C. A. & Telionis, D. P. 1980 Unsteady laminar separation: an experimental study. *J. Fluid Mech.* **97**, 347–384.
Lighthill, M. J. 1954 The response of laminar skin friction and heat transfer to fluctuations in the stream velocity. *Proc. R. Soc. Lond.* A **224**, 1–23.
Maresca, C., Rebont, J. & Valensi, J. 1976 Characteristiques aerodynamiques d'un profil d'aile en mouvement instationnaire. In *14th International Congress of Theoretical and Applied Mechanics, The Netherlands*. Berlin: Springer.
McCroskey, W. J. 1977 Some current research in fluid dynamics. *J. Fluids Engng* **99**, 8–39.
McCroskey, W. J. 1981 The phenomenon of dynamic stall. NASA TM 81264.
McCroskey, W. J. 1982 Unsteady airfoils. *A. Rev. Fluid Mech.* **14**, 285–311.
Messiter, A. F. 1979 Boundary-layer separation. In *Proc. 8th U.S. Nat. Congr. Appl. Mech.*, pp. 157–179. North Hollywood: Western Periodicals.
Messiter, A. F. 1983 Boundary-layer interaction theory. *J. appl. Mech.* **50**, 1104–1113.
Mezaris, T. B. 1979 Visualization and LDV measurements of separating oscillatory laminar flows. M.S. thesis, Virginia Polytechnic Institute and State University.
Mezaris, T. B. & Telionis, D. P. 1980 Separation and the near wake of a pulsating laminar flow. AIAA paper no. 80–1420.
Michalke, A. 1972 The instability of free shear layers. In *Progress in aerospace sciences* (ed. D. Kuchemann), vol. 2, pp. 213–239.
Miksad, R. W., Jones, F. L., Powers, E. J., Kim, Y. C. & Khadra, L. 1982 Experiments on the role of amplitude and phase modulations during transition to turbulence. *J. Fluid Mech.* **123**, 1–29.
Miksad, R. W., Jones, F. L. & Powers, E. J. 1983 Measurements of nonlinear interactions during natural transition of a symmetric wake. *Physics Fluids* **26**, 1402–1409.
Monkewitz, P. & Huerre, P. 1982 The influence of the velocity ratio on the spatial instability of 2-D mixing layers. *Physics Fluids* **25**, 1137–1143.
Moore, F. K. 1957 On the separation of the unsteady laminar boundary layer. In *Boundary layer research* (ed. H. Görtler), pp. 296–311. Berlin: Springer.
Nayfeh, A. H., Ragab, S. A. & Al-Maaitah, A. 1986 Effect of roughness on the stability of boundary layers. AIAA paper no. 86-1044.
Parikh, P. G., Reynolds, W. C., Jayaraman, R. & Carr, L. W. 1981 Dynamic behavior of an unsteady turbulent boundary layer. In *Unsteady turbulent shear flows* (ed. R. Michel, J. Cousteix & R. Houdeville), pp. 35–46. Berlin: Springer.
Prandtl, L. 1904 Über Flüssigkeitsbewegung bei sehr kleiner Reiburg. In *3rd Int. Math. Congress, Heidelberg*, pp. 484–491. Leipzig: Teubner.
Rott, N. 1956 Unsteady viscous flow in the vicinity of a stagnation point. *Q. Jl. appl. Math.* **13**, 444–451.
Ruiter, G. H., Nagib, H. M. & Fejer, A. A. 1971 Unsteady boundary-layer separation over oscillating airfoils. In *Fluid dynamics of unsteady, three-dimensional and separated flows* (ed. F. J. Marshall), pp. 423–426. Lafayette, Indiana: Purdue University.
Sears, W. R. 1956 Some recent developments in airfoil theory. *J. aeronaut. Sci.* **23**, 490–499.
Sears, W. R. & Telionis, D. P. 1975 Boundary layer separation in unsteady flow. *SIAM Jl appl. Math.* **28**, 215–235.
Shen, S. F. 1978 Unsteady separation according to the boundary layer equation. *Adv. appl. Mech.* **18**, 177–220.
Shiloh, K., Shivaprasad, B. G. & Simpson, R. L. 1981 The structure of a separating turbulent boundary layer. Part 3. Transverse velocity measurements. *J. Fluid Mech.* **113**, 75–90.
Simpson, R. L., Strickland, J. H. & Barr, P. W. 1977 Features of a separating turbulent boundary layer in the vicinity of separation. *J. Fluid Mech.* **79**, 553–594.
Simpson, R. L. 1977 Features of unsteady turbulent boundary layers as revealed from experiments. In *Unsteady aerodynamics*. AGARD-CP-227, paper no. 22.

PHILOSOPHICAL TRANSACTIONS OF THE ROYAL SOCIETY A MATHEMATICAL, PHYSICAL & ENGINEERING SCIENCES

Simpson, R. L., Chew, Y. T. & Shivaprasad, B. G. 1981*a* The structure of a separating turbulent boundary layer. Part 1. Mean flow and Reynolds stress. *J. Fluid Mech.* **113**, 23–51.

Simpson, R. L., Chew, Y. T. & Shivaprasad, B. G. 1981*b* The structure of a separating turbulent boundary layer. Part 2. Higher-order turbulence results. *J. Fluid Mech.* **113**, 53–73.

Smith, F. T. 1977 The laminar separation of an incompressible fluid streaming past a smooth surface. *Proc. R. Soc. Lond.* A **356**, 443–463.

Smith, F. T. 1979 Laminar flow of an incompressible fluid past a bluff body: the separation, reattachment, eddy properties and drag. *J. Fluid Mech.* **92**, 171–205.

Smith, F. T. 1985*a* A structure for laminar flow past a bluff body at high Reynolds number. *J. Fluid Mech.* **155**, 175–191.

Smith, F. T. 1985*b* Nonlinear effects and non-parallel flows; the collapse of separating motion, United Technical Research Centre, Hartford, Connecticut, report no. 85-55.

Smith, F. T. 1986 Steady and unsteady boundary-layer separation. *A. Rev. Fluid Mech.* **18**, 197–220.

Smith, F. T. & Bodonyi, R. J. 1985 On short-scale inviscid instabilities in flow past surface-mounted obstacles and other non-parallel motions. *Aeronaut. J.* **89**, 205–212.

Stansby, P. K. 1976 The locking-on of vortex shedding to the cross-stream vibration of circular cylinders in uniform and shear flow. *J. Fluid Mech.* **74**, 641–665.

Stewartson, K. 1974 Multistructured boundary layers on flat plates and related bodies. *Adv. appl. Mech.* **14**, 145–239.

Stuart, J. T. 1971 Unsteady boundary layers. In *Recent research of unsteady boundary layers* (ed. E. A. Eichelbrenner), vol. 1, pp. 1–46. Quebec: Les presses de l'Université Laval.

Sychev, V. V. 1972 On laminar separation. *Fluid Dynam.* **7**, 407.

Sychev, Vik. V. 1979 Asymptotic theory of nonstationary separation. *Fluid Dynam.* **14**, 829–838.

Telionis, D. P. & Koromilas, C. P. 1978 Flow visualization of transient and oscillatory separating laminar flows. In *Nonsteady fluid dynamics* (ed. D. E. Crow & J. A. Miller), pp. 23–32. New York: ASME.

Telionis, D. P. 1979 Review – unsteady boundary layers, separated and attached. *J. Fluids Engng* **101**, 29–43.

Telionis, D. P. 1980 Analytical methods for the prediction of unsteady laminar boundary layers. AGARD short course on unsteady aerodynamics.

Telions, D. P. 1981 *Unsteady viscous flow*. New York, Heidelberg, Berlin: Springer.

Varty, R. L. & Currie, I. G. 1984 Measurements near a laminar separation point. *J. Fluid Mech.* **138**, 1–19.

Williams, J. C. 1977 Incompressible boundary layer separation. In *Annual review of fluid mechanics* (ed. M. Van Dyke, J. V. Wehausen & J. L. Lumley), vol. 9, pp. 177–220.

Winant, C. D. & Browand, F. K. 1974 Vortex pairing: the mechanism of turbulent mixing layer growth at moderate Reynolds numbers. *J. Fluid Mech.* **63**, 237–255.

PHILOSOPHICAL TRANSACTIONS OF THE ROYAL SOCIETY A MATHEMATICAL, PHYSICAL & ENGINEERING SCIENCES

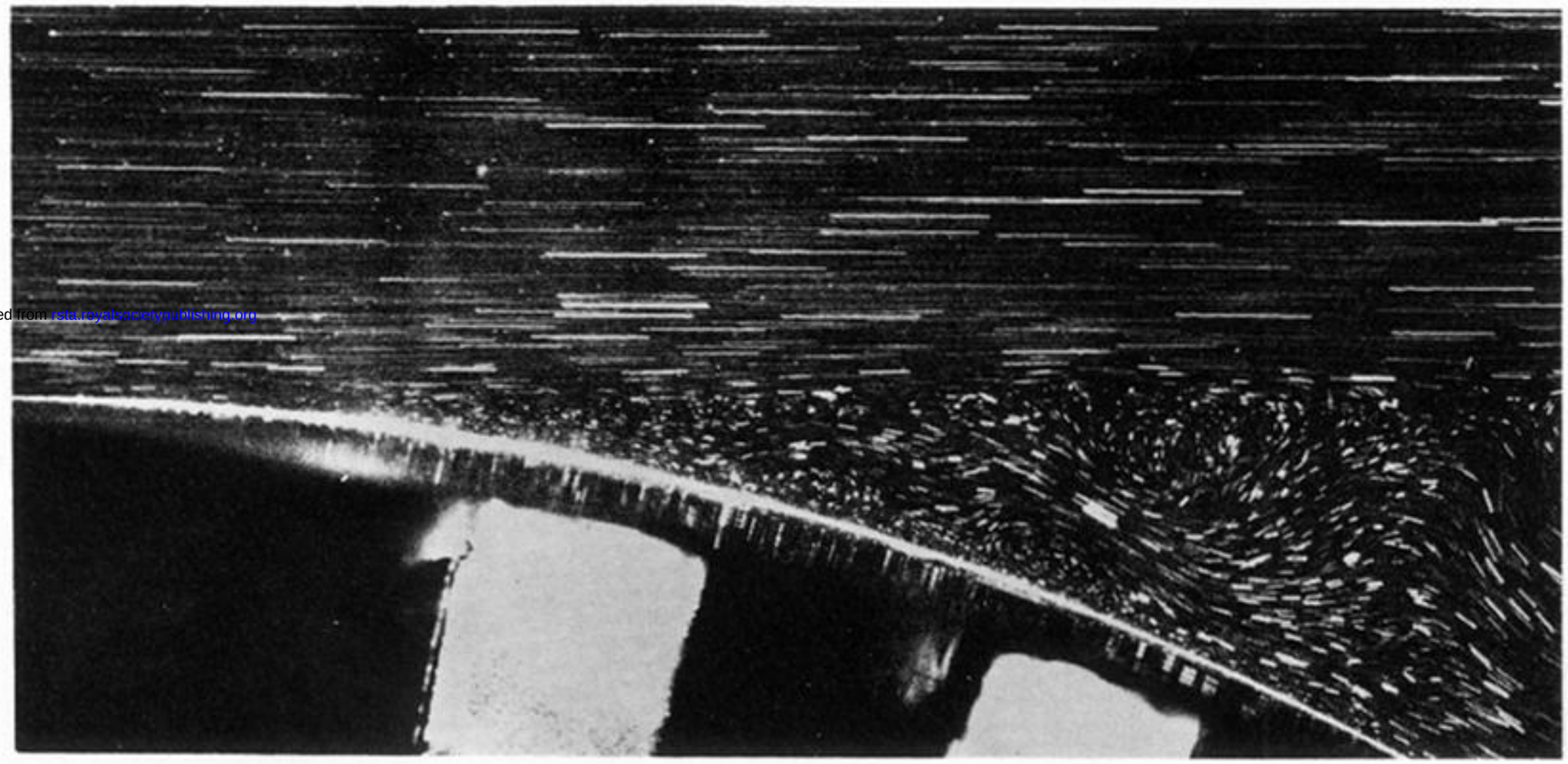

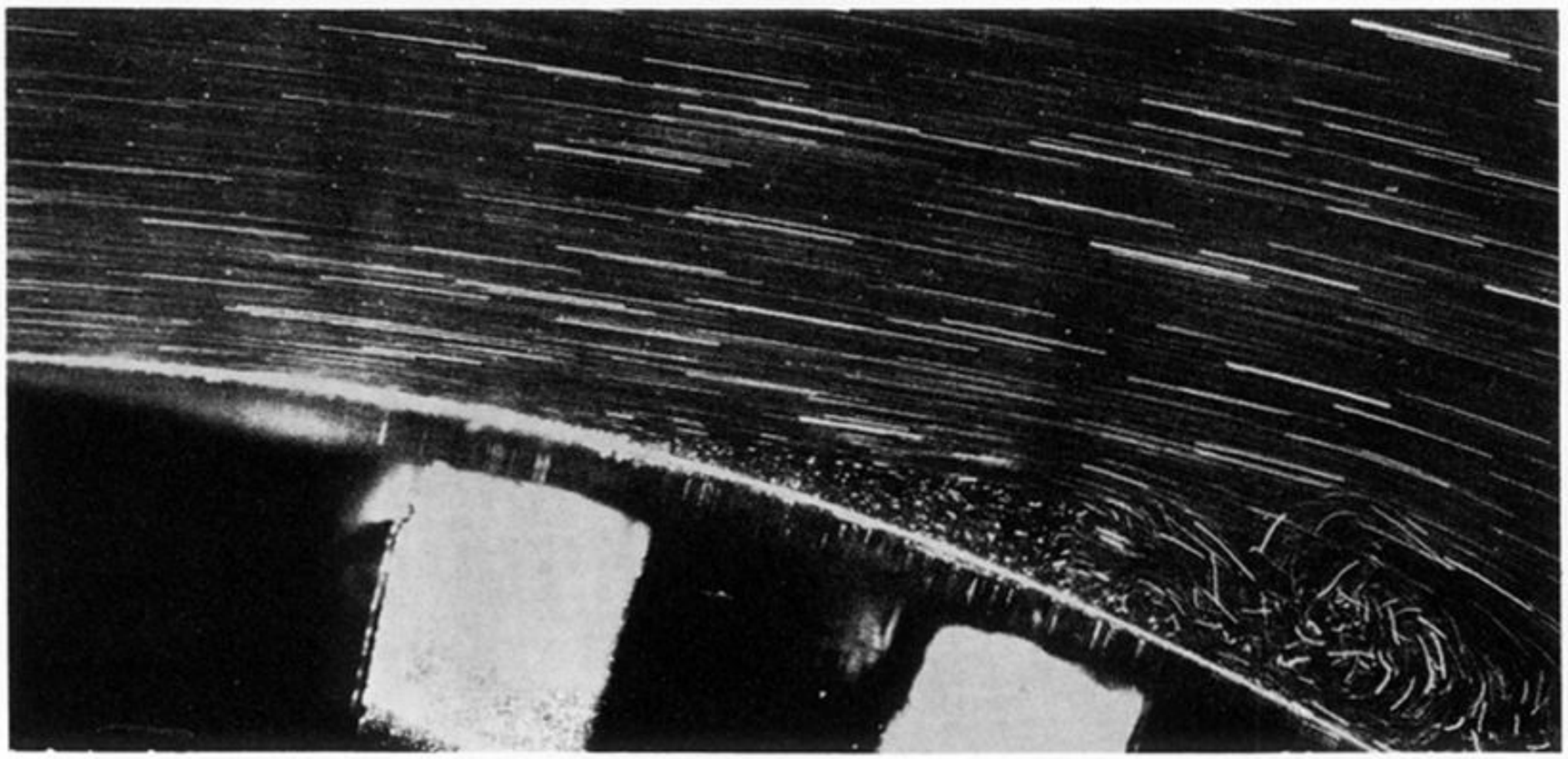

GURE 10. Flow visualization for extreme positions of the flap. Steady case with flap arrangement corresponding to $f_d = 0.2$ Hz. Top: position I; bottom: position II.

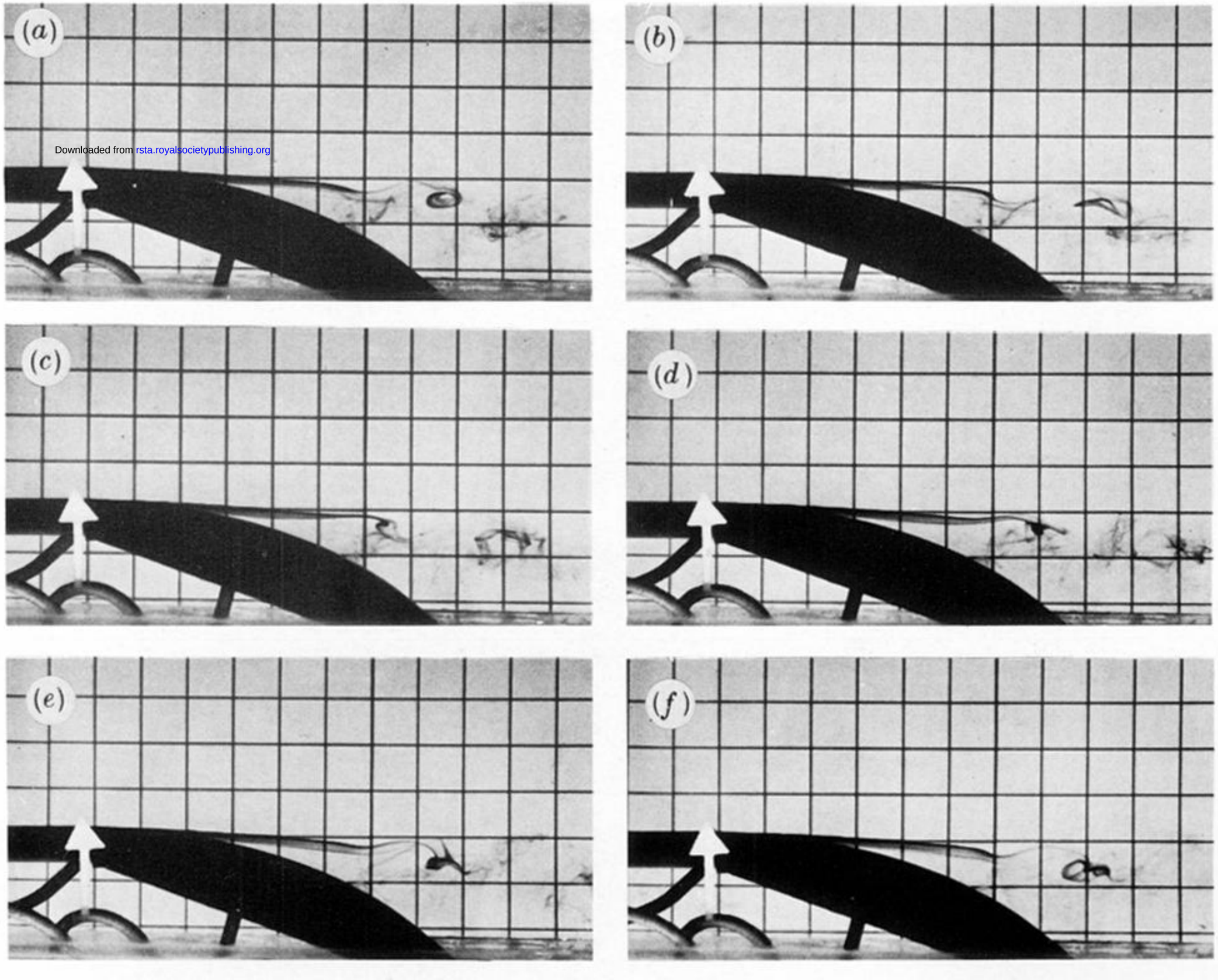

GURE 14. Dye-flow visualization for undisturbed flow at $U_\infty = 8$ cm s^{-1}. (*a*) $t = 0.0$; (*b*) $t = 0.43$; (*c*) $t = 0.86$; (*d*) $t = 1.29$; (*e*) $t = 1.72$; (*f*) $t = 2.15$.

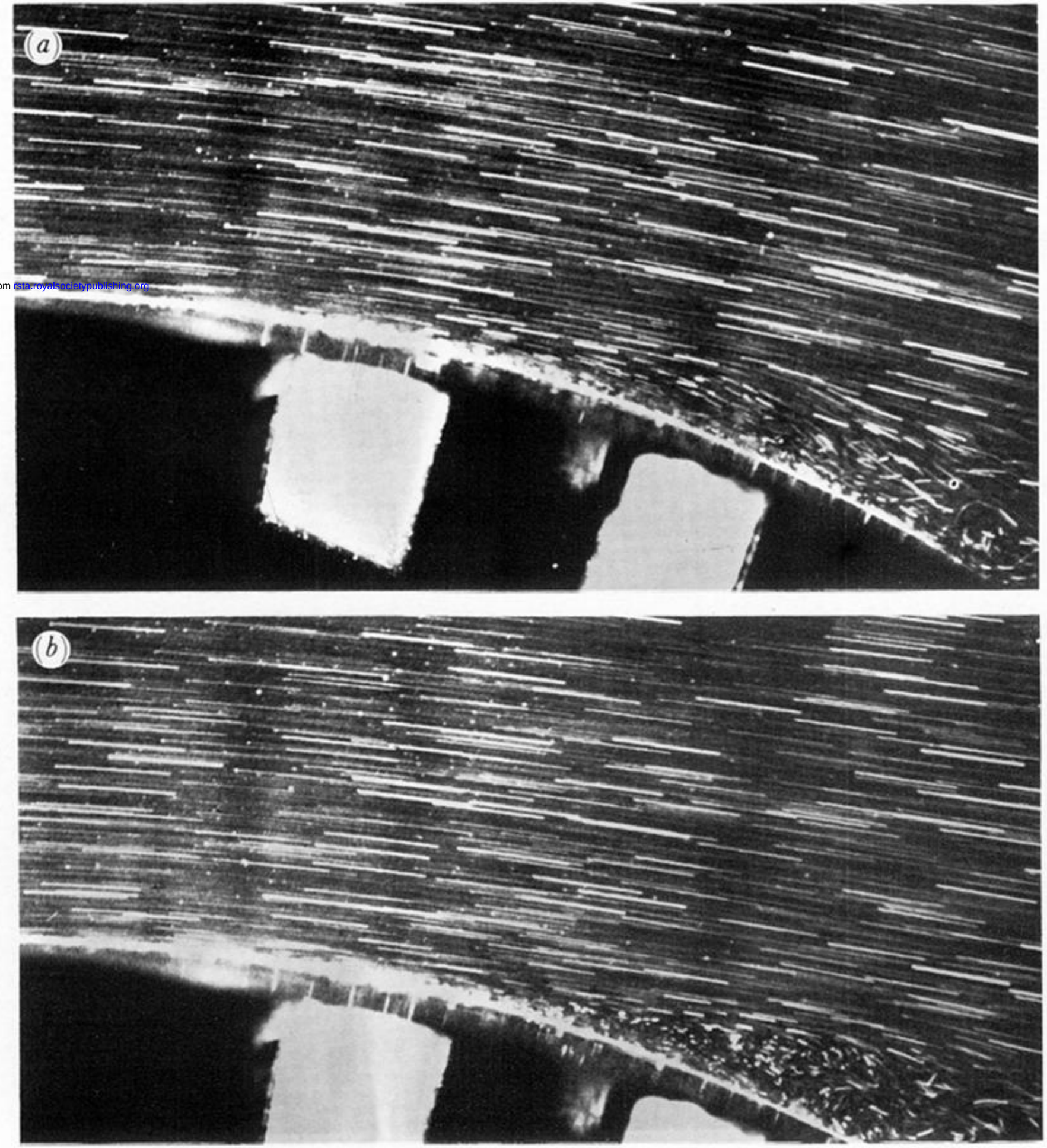

IGURE 18*a*, *b*. Flow visualization of small intervals within one period, T, for $f_d = 0.2$ Hz. (*a*) $t = 0$; (*b*) $t = \frac{1}{10}T$.

PHILOSOPHICAL TRANSACTIONS OF THE ROYAL SOCIETY A MATHEMATICAL, PHYSICAL & ENGINEERING SCIENCES

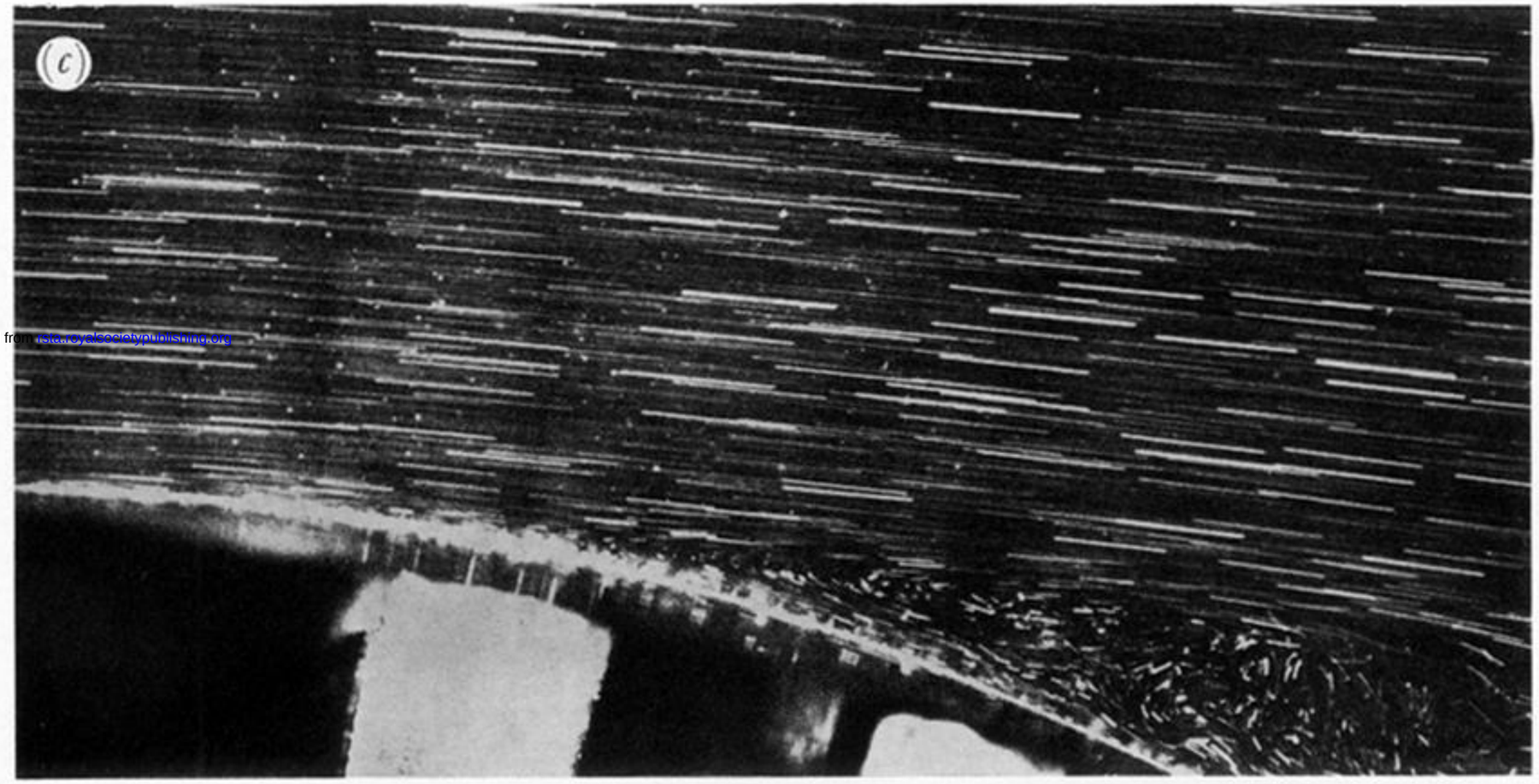

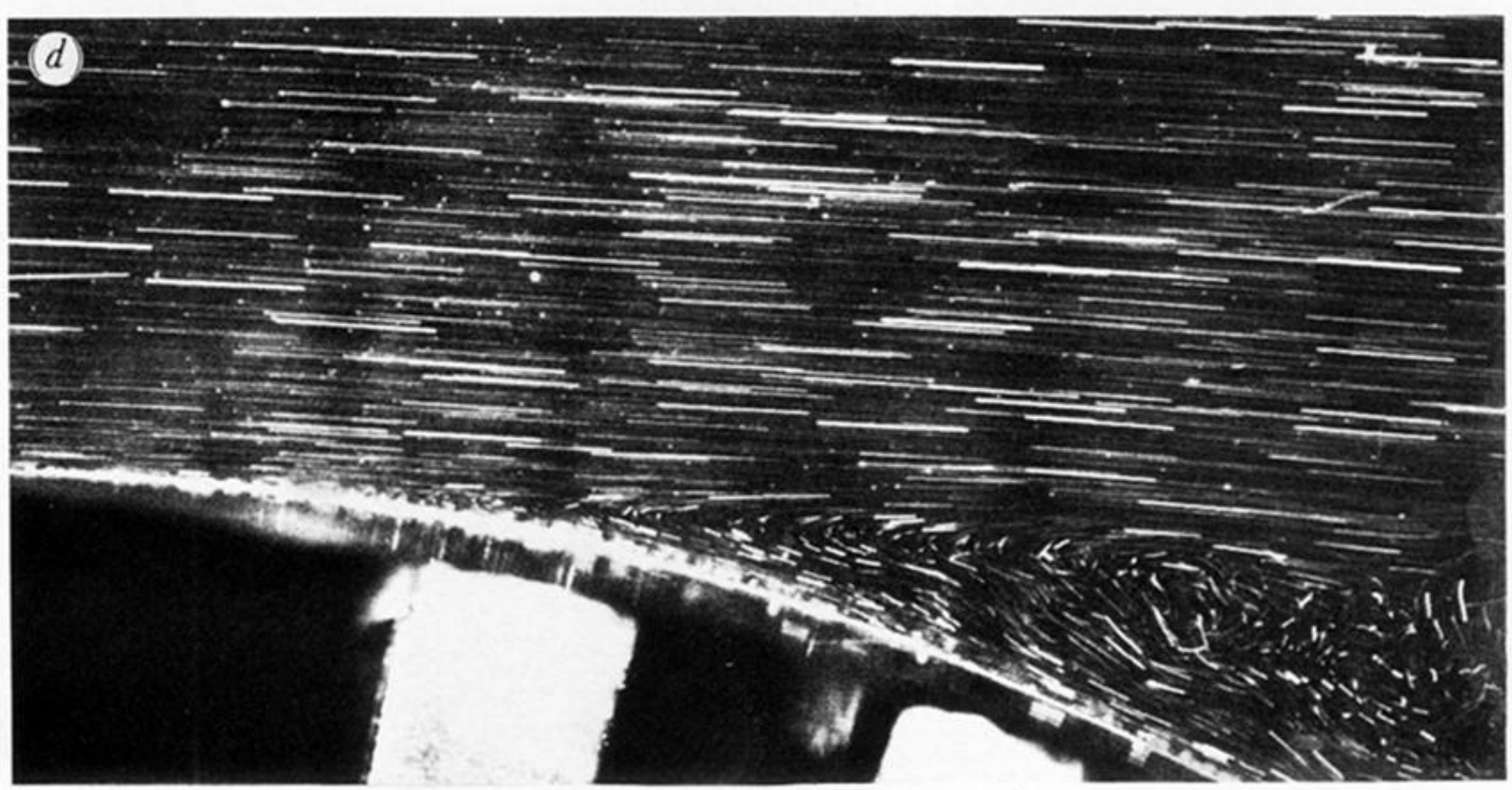

FIGURE 18*c*, *d*. Flow visualization of small intervals within one period, T, for $f_d = 0.2$ Hz. (*c*) $t = \frac{2}{10}T$; (*d*) $t = \frac{3}{10}T$.

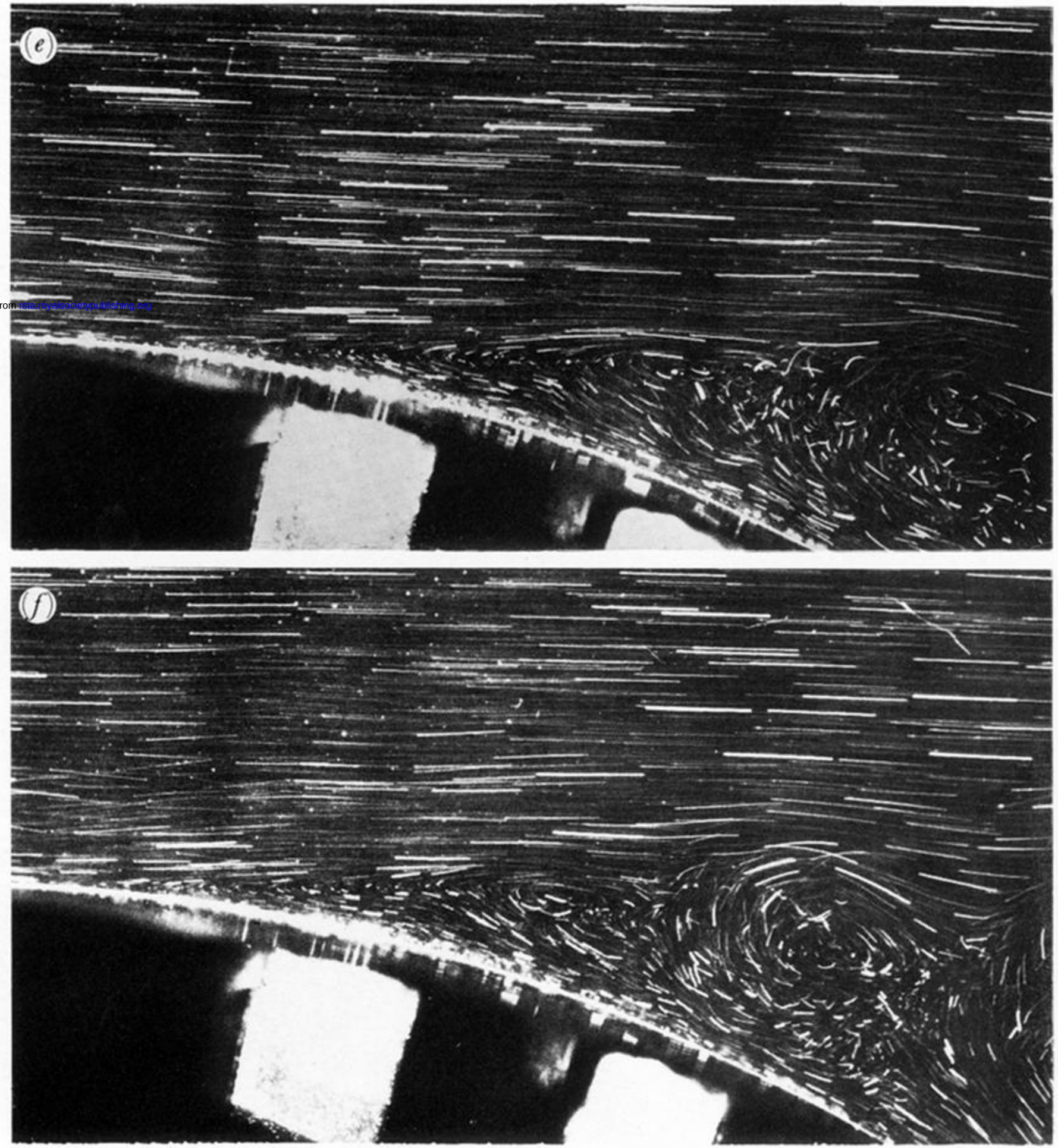

FIGURE 18*e*,*f*. Flow visualization of small intervals within one period, T, for $f_d = 0.2$ Hz. (*e*) $t = \frac{4}{10}T$; (*f*) $t = \frac{5}{10}T$.

PHILOSOPHICAL TRANSACTIONS OF THE ROYAL SOCIETY A MATHEMATICAL, PHYSICAL & ENGINEERING SCIENCES

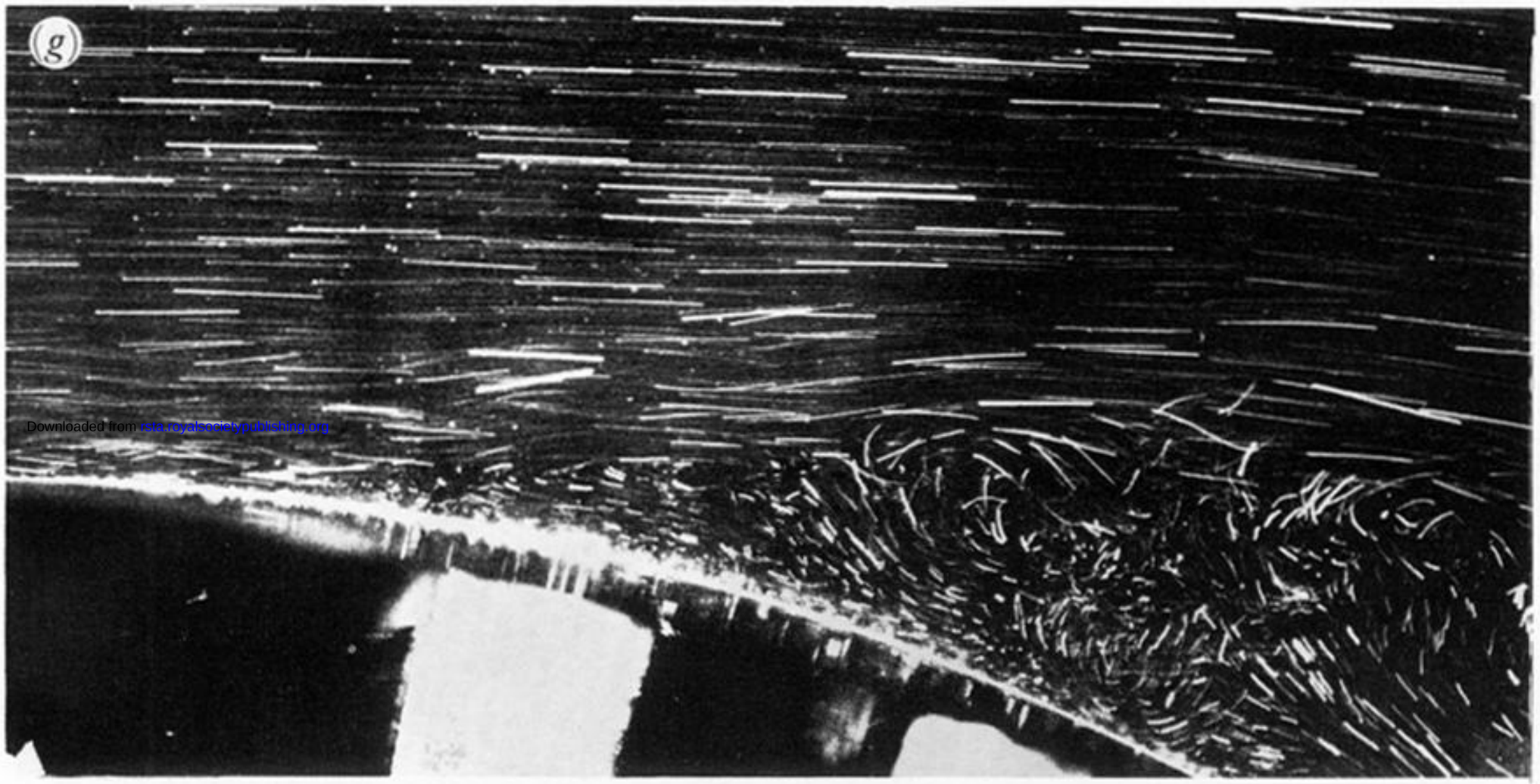

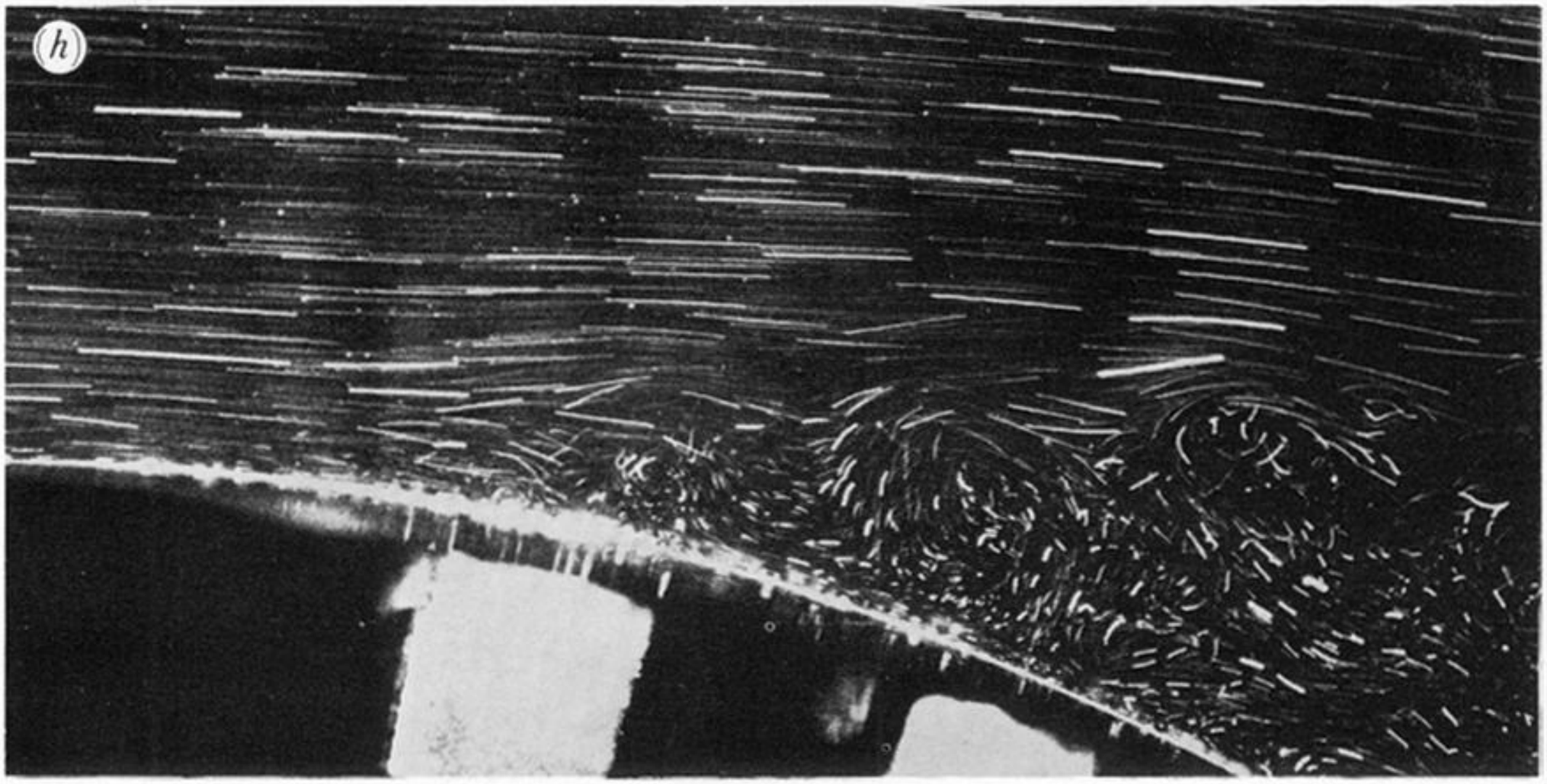

FIGURE 18*g*, *h*. Flow visualization of small intervals within one period, T, for $f_d = 0.2$ Hz. (*g*) $t = \frac{6}{10}T$; (*h*) $t = \frac{7}{10}T$.

PHILOSOPHICAL TRANSACTIONS OF THE ROYAL SOCIETY A MATHEMATICAL, PHYSICAL & ENGINEERING SCIENCES

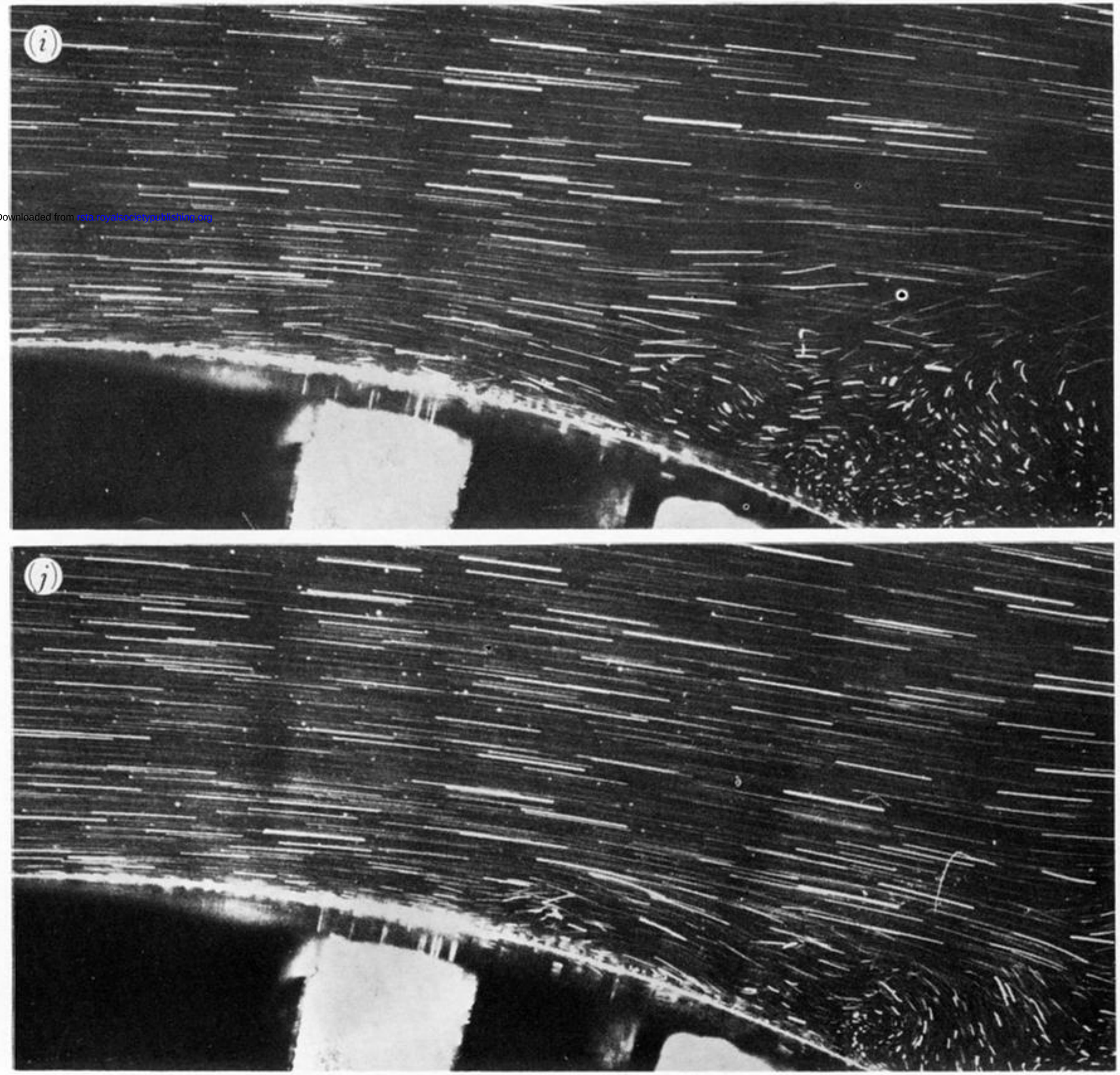

IGURE 18*i*,*j*. Flow visualization of small intervals within one period, T, for $f_d = 0.2$ Hz. (*i*) $t = \frac{8}{10}T$; (*j*) $t = \frac{9}{10}T$.

PHILOSOPHICAL TRANSACTIONS OF THE ROYAL SOCIETY A MATHEMATICAL, PHYSICAL & ENGINEERING SCIENCES

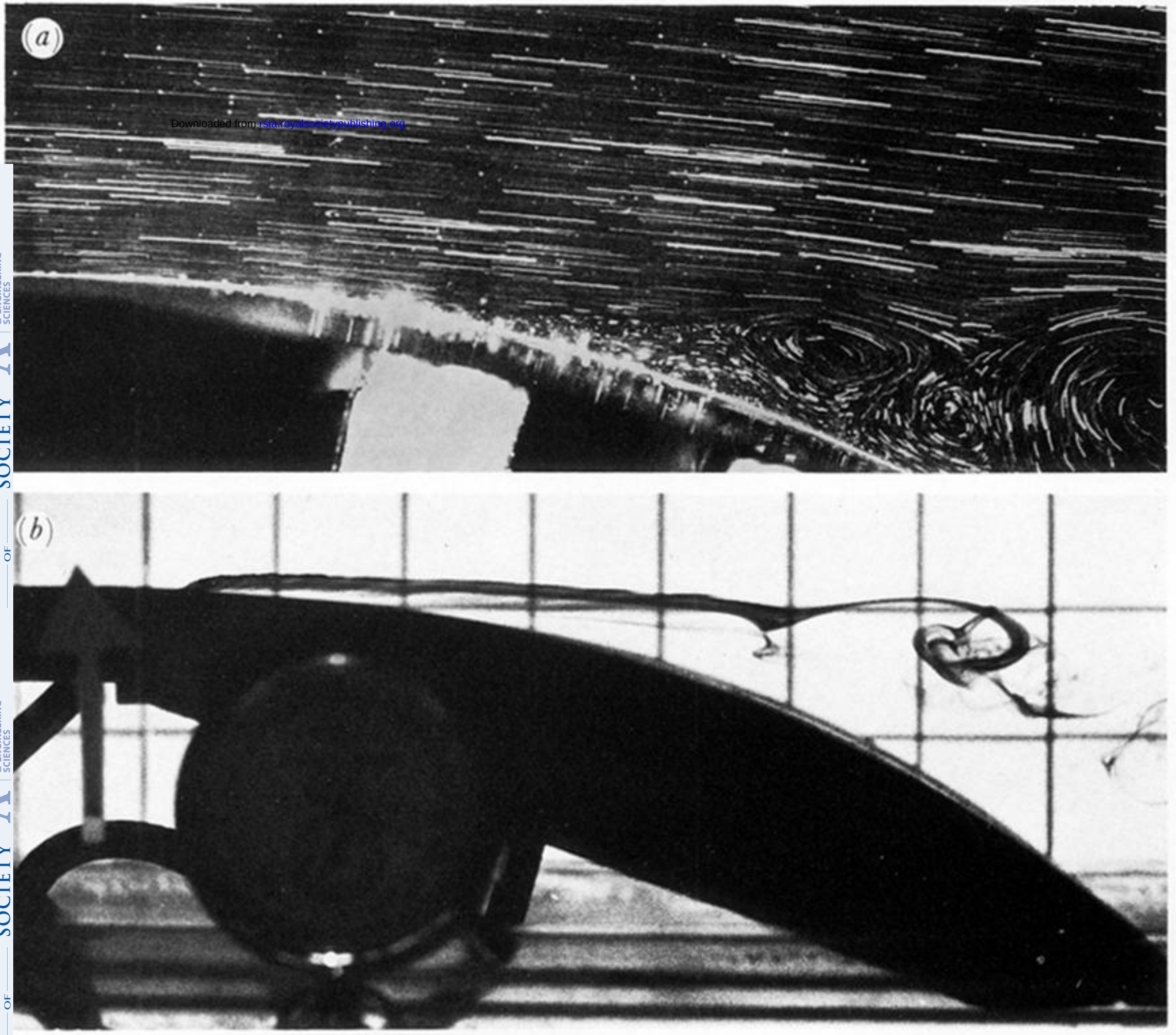

FIGURE 33. Comparison of (*a*) streamlines and (*b*) streaklines.